

IID Sampling from Intractable Distributions

Sourabh Bhattacharya

Indian Statistical Institute

Corresponding email: bhsourabh@gmail.com ¹

Abstract

In this article, we propose a novel methodology for drawing *iid* realizations from any target distribution on the d -dimensional Euclidean space, for any $d \geq 1$. No assumption of compact support is required for the validity of our theory or method. The key idea is to construct an infinite sequence of concentric closed ellipsoids, motivated by the insight that the central ellipsoid tends to capture the modal region, while the regions between successive ellipsoids (ellipsoidal annuli) increasingly represent the tail regions of the distribution.

Representing the target distribution as an infinite mixture of component distributions defined on the central ellipsoid and the annuli, we propose a simulation strategy in which a component is first selected with its mixing probability, and then sampled exactly using perfect simulation. The perfect sampling scheme is built upon a minorization inequality for the general Metropolis–Hastings algorithm driven by uniform proposal distributions on the compact ellipsoid and annuli.

Unlike most existing work on perfect sampling, our method is not only theoretically valid but also practically applicable to any target distribution on \mathbb{R}^d , and is readily parallelizable. We validate the practicality of our approach by generating 10,000 *iid* realizations from standard distributions such as the normal, Student's t with 5 degrees of freedom, and Cauchy, for dimensions $d = 1, 5, 10, 50, 100$, as well as from a 50-dimensional normal mixture distribution. In all cases, implementation times are reasonable, often less than a minute in our parallel setup, and the results are highly accurate.

We further demonstrate the method by generating 10,000 *iid* realizations from posterior distributions associated with the well-known Challenger data, a Salmonella dataset, and a 160-dimensional spatial example of radionuclide count data on Rongelap Island. In each case, the results are encouraging and computation times remain very reasonable.

AMS (2000) subject classification Primary: 65C05; 62F15; Secondary: 60J22; 65C40; 62H20; 68W10.

Keywords: Ellipsoid; Minorization; Parallel computing; Perfect sampling; Residual distribution; Transformation-based Markov Chain Monte Carlo.

¹This article is intended for Dr. C. R. Rao Special Issue.

1 Introduction

That Markov Chain Monte Carlo (MCMC) has revolutionized Bayesian computation is an understatement. Yet, despite its impact, MCMC has faced renewed scrutiny due to persistent convergence assessment challenges. Even the most experienced MCMC theorists and practitioners often resort to deterministic or ad-hoc approximations to posterior distributions, considering the difficulties of diagnosing convergence insurmountable.

The concept of perfect simulation, introduced by [Propp and Wilson \(1996\)](#), initially appeared promising to the MCMC community as a solution to the convergence problem. However, the apparent infeasibility of direct practical implementation in general Bayesian problems led to skepticism and, in many cases, outright disbelief. For instance, when the article by [Mukhopadhyay and Bhattacharya \(2012\)](#) on perfect sampling in mixture contexts was submitted to a reputed journal, reviewers rejected it, deeming the idea overly ambitious. To our knowledge, little promising research on perfect sampling has appeared in recent years.

In this article, we address the task of producing *iid* realizations from any target distribution on \mathbb{R}^d , with $d \geq 1$, where \mathbb{R} is the real line. Our key idea is to construct an infinite sequence of closed ellipsoids and represent the target distribution as an infinite mixture on the central ellipsoid and the annuli between successive ellipsoids. This construction reflects our insight that the central ellipsoid essentially captures the modal region, while the annuli represent the tail regions of the target distribution.

Our proposal for generating *iid* realizations involves selecting a mixture component with its mixing probability and then simulating exactly from the chosen component using a perfect sampling scheme. To develop this scheme, we first consider the general Metropolis–Hastings algorithm on compact ellipsoids and annuli, driven by uniform proposal distributions. Exploiting compactness, we derive a suitable minorization inequality for each set in the sequence. Representing the Metropolis–Hastings chain as a mixture of two components, we then construct a perfect sampler for the density on its relevant support. Moreover, by adopting and rectifying an idea proposed in Murdoch and Green (1998), we avoid the computationally expensive coupling from the past (CFTP) algorithm of [Propp and Wilson \(1996\)](#). Bypassing CFTP makes our approach computationally feasible. Integrating these ideas, we develop a generic parallel algorithm for simulating *iid* realizations from general target distributions.

To illustrate the feasibility of our methodology, we apply the parallel algorithm to several standard distributions: normal, Student’s *t* with 5 degrees of freedom, and Cauchy, for $d = 1, 5, 10, 50, 100$. We also consider a 50-dimensional mixture of normal distributions. In all cases, we simulate 10,000 *iid* realizations, and the results are highly accurate. Furthermore, computation times are reasonable, with several experiments completing in less than a minute.

We also apply our method to posterior distributions based on real data. Specifically, we generate 10,000 *iid* realizations from the posteriors corresponding to the Challenger data and the Salmonella data, with two and three parameters respectively. Finally, we address a particularly challenging case: generating 10,000 *iid* realizations from the 160-dimensional posterior distribution for radionuclide count data on Rongelap Island, a problem widely regarded as difficult for MCMC convergence. Remarkably, we obtain *iid* samples within 30 minutes, and the results are highly reliable.

The remainder of the article is organized as follows. Section 2 introduces our key idea. Section 3 develops the set-wise perfect sampling theory and method. Section 4

presents our complete parallel algorithm for *iid* sampling from general target distributions. Section 5 reports simulation experiments with standard univariate and multivariate distributions, while Section 6 details applications to posterior distributions based on real data. Finally, Section 7 provides concluding remarks.

2 The *iid* sampling idea

Let $\pi(\boldsymbol{\theta})$ be the target distribution supported on \mathbb{R}^d , where $d \geq 1$. Here $\boldsymbol{\theta} = (\theta_1, \dots, \theta_d)^T$. Note that the distribution can be represented as

$$\pi(\boldsymbol{\theta}) = \sum_{i=1}^{\infty} \pi(\mathbf{A}_i) \pi_i(\boldsymbol{\theta}), \quad (1)$$

where \mathbf{A}_i are disjoint compact subsets of \mathbb{R}^d such that $\cup_{i=1}^{\infty} \mathbf{A}_i = \mathbb{R}^d$, and

$$\pi_i(\boldsymbol{\theta}) = \frac{\pi(\boldsymbol{\theta})}{\pi(\mathbf{A}_i)} I_{\mathbf{A}_i}(\boldsymbol{\theta}), \quad (2)$$

is the distribution of $\boldsymbol{\theta}$ restricted on \mathbf{A}_i ; $I_{\mathbf{A}_i}$ being the indicator function of \mathbf{A}_i . In (1), $\pi(\mathbf{A}_i) = \int_{\mathbf{A}_i} \pi(d\boldsymbol{\theta}) \geq 0$. Clearly, $\sum_{i=1}^{\infty} \pi(\mathbf{A}_i) = 1$.

The key idea of generating *iid* realizations from $\pi(\boldsymbol{\theta})$ is to randomly select π_i with probability $\pi(\mathbf{A}_i)$ and then to perfectly simulate from π_i .

2.1 Choice of the sets \mathbf{A}_i

For some appropriate d -dimensional vector $\boldsymbol{\mu}$ and $d \times d$ positive definite scale matrix $\boldsymbol{\Sigma}$, we shall set $\mathbf{A}_i = \{\boldsymbol{\theta} : c_{i-1} \leq (\boldsymbol{\theta} - \boldsymbol{\mu})^T \boldsymbol{\Sigma}^{-1} (\boldsymbol{\theta} - \boldsymbol{\mu}) \leq c_i\}$ for $i = 1, 2, \dots$, where $0 = c_0 < c_1 < c_2 < \dots$. Note that $\mathbf{A}_1 = \{\boldsymbol{\theta} : (\boldsymbol{\theta} - \boldsymbol{\mu})^T \boldsymbol{\Sigma}^{-1} (\boldsymbol{\theta} - \boldsymbol{\mu}) \leq c_1\}$, and for $i \geq 2$, $\mathbf{A}_i = \{\boldsymbol{\theta} : (\boldsymbol{\theta} - \boldsymbol{\mu})^T \boldsymbol{\Sigma}^{-1} (\boldsymbol{\theta} - \boldsymbol{\mu}) \leq c_i\} \setminus \cup_{j=1}^{i-1} \mathbf{A}_j$. Observe that ideally one should set $\mathbf{A}_i = \{\boldsymbol{\theta} : c_{i-1} < (\boldsymbol{\theta} - \boldsymbol{\mu})^T \boldsymbol{\Sigma}^{-1} (\boldsymbol{\theta} - \boldsymbol{\mu}) \leq c_i\}$, but since $\boldsymbol{\theta}$ has continuous distribution in our setup, we shall continue with $\mathbf{A}_i = \{\boldsymbol{\theta} : c_{i-1} \leq (\boldsymbol{\theta} - \boldsymbol{\mu})^T \boldsymbol{\Sigma}^{-1} (\boldsymbol{\theta} - \boldsymbol{\mu}) \leq c_i\}$.

Thus, the first member of the sequence of sets \mathbf{A}_i ; $i \geq 1$, is a closed ellipsoid, while the others are closed annuli, the regions between two successive concentric closed ellipsoids. The compact ellipsoid \mathbf{A}_1 tends to support the modal region of the target distribution π and for increasing $i \geq 2$, the compact annuli \mathbf{A}_i tend to support the tail regions of the target distribution. Thus in practice, it is useful to choose $\sqrt{c_1}$ associated with \mathbf{A}_1 to be relatively large compared to $\sqrt{c_i}$ for $i \geq 2$. As will be seen in Section 2.3.1, for $i \geq 1$, $\sqrt{c_i}$ are the radii of d -dimensional balls of the form $\{\mathbf{Y} : \mathbf{Y}^T \mathbf{Y} \leq c_i\}$ which has linear correspondence with d -dimensional ellipsoids of the form $\{\boldsymbol{\theta} : (\boldsymbol{\theta} - \boldsymbol{\mu})^T \boldsymbol{\Sigma}^{-1} (\boldsymbol{\theta} - \boldsymbol{\mu}) \leq c_i\}$. Hence, we shall refer to $\sqrt{c_i}$; $i \geq 1$, as radii.

2.2 Choice of $\boldsymbol{\mu}$ and $\boldsymbol{\Sigma}$

Theoretically, any choice of $\boldsymbol{\mu} \in \mathbb{R}^d$ and any $d \times d$ positive definite scale matrix $\boldsymbol{\Sigma}$ is valid for our method. However, judicious choices of $\boldsymbol{\mu}$ and $\boldsymbol{\Sigma}$ play important roles in the efficiency of our *iid* algorithm. In this regard, in practice, $\boldsymbol{\mu}$ and $\boldsymbol{\Sigma}$ will be the estimates of the mean (if it exists, or co-ordinate-wise median otherwise) and covariance structure of π (if it exists, or some appropriate scale matrix otherwise). These estimates will be assumed

to be obtained from some reliably implemented efficient MCMC algorithm. In this regard, we recommend the transformation based Markov Chain Monte Carlo (TMCMC) methodology introduced by [Dutta and Bhattacharya \(2014\)](#) that simultaneously updates all the variables using suitable deterministic transformations of some low-dimensional (often one-dimensional) random variable defined on some relevant support. Since the method is driven by the low-dimensional random variable, this leads to drastic dimension reduction in effect, with great improvement in acceptance rates and computational efficiency, while ensuring adequate convergence properties. Our experiences also reveal that addition of a further deterministic step to TMCMC, in a similar vein as in [Liu and Sabatti \(2000\)](#) often dramatically enhances the convergence properties of TMCMC.

2.3 Dealing with the mixing probabilities $\pi(\mathbf{A}_i)$

Recall that the key idea of *iid* sampling from $\pi(\boldsymbol{\theta})$ is to randomly select π_i with probability $\pi(\mathbf{A}_i)$ and then to exactly simulate from π_i . However, the mixing probabilities $\pi(\mathbf{A}_i)$ are not available prior to simulation. Since there are infinite number of such probabilities, even estimation of all these probabilities using only a finite TMCMC sample from π is out of the question. But estimation of $\pi(\mathbf{A}_i)$ using Monte Carlo samples drawn uniformly from \mathbf{A}_i makes sense, and the strategy applies to all $i \geq 1$. For the time being assume that we have an infinite number of parallel processors, and the i -th processor is used to estimate $\pi(\mathbf{A}_i)$ using Monte Carlo sampling up to a constant. To elaborate, let $\pi(\boldsymbol{\theta}) = C\tilde{\pi}(\boldsymbol{\theta})$, where $C > 0$ is the unknown normalizing constant. Then for any Borel set \mathbf{A} in the Borel σ -field of \mathbb{R}^d , letting $\mathcal{L}(\mathbf{A})$ denote the Lebesgue measure of \mathbf{A} , observe that

$$\pi(\mathbf{A}_i) = C\mathcal{L}(\mathbf{A}_i) \int \tilde{\pi}(\boldsymbol{\theta}) \frac{1}{\mathcal{L}(\mathbf{A}_i)} I_{\mathbf{A}_i}(\boldsymbol{\theta}) d\boldsymbol{\theta} = C\mathcal{L}(\mathbf{A}_i) E[\tilde{\pi}(\boldsymbol{\theta})], \quad (3)$$

the right hand side being $C\mathcal{L}(\mathbf{A}_i)$ times the expectation of $\tilde{\pi}(\boldsymbol{\theta})$ with respect to the uniform distribution on \mathbf{A}_i . This expectation can be estimated by generating realizations of $\boldsymbol{\theta}$ from the uniform distribution on \mathbf{A}_i , evaluating $\tilde{\pi}(\boldsymbol{\theta})$ for the realizations and taking their average. Let $\widehat{\tilde{\pi}(\mathbf{A}_i)}$ denote the Monte Carlo average times $\mathcal{L}(\mathbf{A}_i)$, so that $\widehat{\tilde{\pi}(\mathbf{A}_i)}$ is an estimate of $\tilde{\pi}(\mathbf{A}_i)$. The required uniform sample generation from \mathbf{A}_i and computation of $\mathcal{L}(\mathbf{A}_i)$ can be achieved in straightforward ways, which we elucidate below.

2.3.1 Uniform sampling from \mathbf{A}_i

First consider uniform generation from the d -dimensional ball $\{\mathbf{Y} : \mathbf{Y}^T \mathbf{Y} \leq c_1\}$, which consists of generation of $X_k \stackrel{iid}{\sim} N(0, 1)$, for $k = 1, \dots, d$, $U \sim U(0, 1)$, the uniform distribution on $[0, 1]$, and setting $\mathbf{Y} = \sqrt{c_1} U^{1/d} \mathbf{X} / \|\mathbf{X}\|$, where $\mathbf{X} = (X_1, \dots, X_d)^T$ and $\|\cdot\|$ is the Euclidean norm. Then, letting $\boldsymbol{\Sigma} = \mathbf{B}\mathbf{B}^T$, where \mathbf{B} is the lower triangular Cholesky factor of $\boldsymbol{\Sigma}$, $\boldsymbol{\theta} = \boldsymbol{\mu} + \mathbf{B}\mathbf{Y}$ is a uniform realization from \mathbf{A}_1 . To generate uniformly from $\mathbf{A}_i = \{\boldsymbol{\theta} : c_{i-1} \leq (\boldsymbol{\theta} - \boldsymbol{\mu})^T \boldsymbol{\Sigma}^{-1} (\boldsymbol{\theta} - \boldsymbol{\mu}) \leq c_i\} = \{\boldsymbol{\theta} : (\boldsymbol{\theta} - \boldsymbol{\mu})^T \boldsymbol{\Sigma}^{-1} (\boldsymbol{\theta} - \boldsymbol{\mu}) \leq c_i\} \setminus \{\boldsymbol{\theta} : (\boldsymbol{\theta} - \boldsymbol{\mu})^T \boldsymbol{\Sigma}^{-1} (\boldsymbol{\theta} - \boldsymbol{\mu}) \leq c_{i-1}\}$ for $i \geq 2$, we shall continue uniform simulation of $\tilde{\boldsymbol{\theta}}$ from $\{\boldsymbol{\theta} : (\boldsymbol{\theta} - \boldsymbol{\mu})^T \boldsymbol{\Sigma}^{-1} (\boldsymbol{\theta} - \boldsymbol{\mu}) \leq c_i\}$ until $\tilde{\boldsymbol{\theta}}$ satisfies $(\tilde{\boldsymbol{\theta}} - \boldsymbol{\mu})^T \boldsymbol{\Sigma}^{-1} (\tilde{\boldsymbol{\theta}} - \boldsymbol{\mu}) > c_{i-1}$.

Note that this basic rejection sampling scheme will be inefficient with high rejection probabilities for $i \geq 2$ when $\sqrt{c_i} - \sqrt{c_{i-1}}$ are very small. In such cases, it is important to replace this algorithm with methods that avoid the rejection mechanism. We indeed devise such a method for situations with small $\sqrt{c_i} - \sqrt{c_{i-1}}$ for $i \geq 2$ that completely bypasses rejection sampling; see Section 6.

2.3.2 Lebesgue measure of \mathbf{A}_i

It is well-known (see, for example, Giraud (2015)) that the volume of a d -dimensional ball of radius c is given by $\frac{\pi^{d/2}}{\Gamma(d/2+1)}c^d$, where $\Gamma(x) = \int_0^\infty t^{x-1} \exp(-t)dt$, for $x > 0$, is the Gamma function. Hence, in our case, letting $|\mathbf{B}|$ denote the determinant of \mathbf{B} ,

$$\mathcal{L}(\mathbf{A}_1) = |\mathbf{B}| \times \mathcal{L}(\{\boldsymbol{\theta} : \|\boldsymbol{\theta}\| \leq \sqrt{c_1}\}) = \frac{|\mathbf{B}|\pi^{d/2}}{\Gamma(d/2+1)}c_1^{d/2},$$

and for $i \geq 2$, \mathbf{A}_i has Lebesgue measure

$$\begin{aligned} \mathcal{L}(\mathbf{A}_i) &= |\mathbf{B}| \times \mathcal{L}(\{\boldsymbol{\theta} : \|\boldsymbol{\theta}\| \leq \sqrt{c_i}\}) - |\mathbf{B}| \times \mathcal{L}(\{\boldsymbol{\theta} : \|\boldsymbol{\theta}\| \leq \sqrt{c_{i-1}}\}) \\ &= |\mathbf{B}| \times \frac{\pi^{d/2}}{\Gamma(d/2+1)} (c_i^{d/2} - c_{i-1}^{d/2}). \end{aligned}$$

The aforementioned ideas show that all the estimates $\widehat{\tilde{\pi}(\mathbf{A}_i)}$, for $i \geq 1$, are obtainable simultaneously by parallel processing. Also assume that the Monte Carlo sample size N_i is large enough for each i such that for any $\epsilon > 0$,

$$1 - \epsilon \leq \frac{\widehat{\tilde{\pi}(\mathbf{A}_i)}}{\tilde{\pi}(\mathbf{A}_i)} \leq 1 + \epsilon. \quad (4)$$

We further assume that depending on ϵ , there exists $M_0 \geq 1$ such that for all $M \geq M_0$,

$$1 - \epsilon \leq C \sum_{i=1}^M \widehat{\tilde{\pi}(\mathbf{A}_i)} \leq 1 + \epsilon. \quad (5)$$

Letting

$$\hat{\pi}(\boldsymbol{\theta}) = C \sum_{i=1}^{\infty} \widehat{\tilde{\pi}(\mathbf{A}_i)} \pi_i(\boldsymbol{\theta}), \quad (6)$$

which is a well-defined density due to (5), we next provide a rejection sampling based argument to establish that it is sufficient to perfectly simulate from $\hat{\pi}(\boldsymbol{\theta})$ in order to sample perfectly from $\pi(\boldsymbol{\theta})$.

2.4 A rejection sampling argument for validation of $\hat{\pi}(\boldsymbol{\theta})$

Due to (4), for all $\boldsymbol{\theta} \in \mathbb{R}^d$,

$$\pi(\boldsymbol{\theta}) = C \sum_{i=1}^{\infty} \widehat{\tilde{\pi}(\mathbf{A}_i)} \times \frac{\tilde{\pi}(\mathbf{A}_i)}{\widehat{\tilde{\pi}(\mathbf{A}_i)}} \times \pi_i(\boldsymbol{\theta}) \leq C(1 + \epsilon) \sum_{i=1}^{\infty} \widehat{\tilde{\pi}(\mathbf{A}_i)} \pi_i(\boldsymbol{\theta}) = (1 + \epsilon) \hat{\pi}(\boldsymbol{\theta}).$$

That is, for all $\boldsymbol{\theta} \in \mathbb{R}^d$,

$$\frac{\pi(\boldsymbol{\theta})}{\hat{\pi}(\boldsymbol{\theta})} \leq 1 + \epsilon, \quad (7)$$

showing that rejection sampling is applicable for generating samples from $\pi(\boldsymbol{\theta})$ by sampling $\boldsymbol{\theta}$ from $\hat{\pi}(\boldsymbol{\theta})$ and generating $U \sim U(0, 1)$ until the following is satisfied:

$$U < \frac{\pi(\boldsymbol{\theta})}{(1 + \epsilon)\hat{\pi}(\boldsymbol{\theta})}. \quad (8)$$

In (8), $\boldsymbol{\theta} \in \mathbf{A}_i$ for some $i \geq 1$. Hence, due to (4),

$$\frac{\pi(\boldsymbol{\theta})}{(1+\epsilon)\widehat{\pi}(\boldsymbol{\theta})} = \frac{1}{(1+\epsilon)} \frac{\widehat{\tilde{\pi}}(\mathbf{A}_i)}{\widehat{\tilde{\pi}}(\mathbf{A}_i)} > \frac{1-\epsilon}{1+\epsilon}. \quad (9)$$

The right most side of (9) can be made arbitrarily close to 1 for sufficiently small $\epsilon > 0$. Now, since $U \leq 1$ with probability 1, this entails that (8) is satisfied with probability almost equal to one. Thus, for sufficiently small $\epsilon > 0$, we can safely assume that (8) holds for all practical applications, so that any simulation of $\boldsymbol{\theta}$ from $\widehat{\pi}(\boldsymbol{\theta})$ would be accepted in the rejection sampling step. In other words, to generate samples from the target density $\pi(\boldsymbol{\theta})$ it is sufficient to simply generate from $\widehat{\pi}(\boldsymbol{\theta})$, for sufficiently small ϵ .

3 Perfect sampling from $\widehat{\pi}(\boldsymbol{\theta})$

For perfect sampling from $\widehat{\pi}(\boldsymbol{\theta})$ we first need to select π_i with probability $C\widehat{\tilde{\pi}}(\mathbf{A}_i)$ for some $i \geq 1$, and then need to sample from π_i in the perfect sense. Now π_i would be selected if

$$\frac{\sum_{j=1}^{i-1} \widehat{\tilde{\pi}}(\mathbf{A}_j)}{\sum_{j=1}^{\infty} \widehat{\tilde{\pi}}(\mathbf{A}_j)} < U < \frac{\sum_{j=1}^i \widehat{\tilde{\pi}}(\mathbf{A}_j)}{\sum_{j=1}^{\infty} \widehat{\tilde{\pi}}(\mathbf{A}_j)}, \quad (10)$$

where $U \sim U(0, 1)$ and $\widehat{\tilde{\pi}}(\mathbf{A}_0) = 0$. But the denominator of the left and right hand sides of (10) involves an infinite sum, which can not be computed. However, note that due to (5),

$$1 - \epsilon \leq \frac{\sum_{j=1}^M \widehat{\tilde{\pi}}(\mathbf{A}_j)}{\sum_{j=1}^{\infty} \widehat{\tilde{\pi}}(\mathbf{A}_j)} \leq 1 + \epsilon. \quad (11)$$

The following hold due to (11):

$$(1 - \epsilon) \frac{\sum_{j=1}^{i-1} \widehat{\tilde{\pi}}(\mathbf{A}_j)}{\sum_{j=1}^M \widehat{\tilde{\pi}}(\mathbf{A}_j)} \leq \frac{\sum_{j=1}^{i-1} \widehat{\tilde{\pi}}(\mathbf{A}_j)}{\sum_{j=1}^{\infty} \widehat{\tilde{\pi}}(\mathbf{A}_j)} \leq (1 + \epsilon) \frac{\sum_{j=1}^{i-1} \widehat{\tilde{\pi}}(\mathbf{A}_j)}{\sum_{j=1}^M \widehat{\tilde{\pi}}(\mathbf{A}_j)}; \quad (12)$$

$$(1 - \epsilon) \frac{\sum_{j=1}^i \widehat{\tilde{\pi}}(\mathbf{A}_j)}{\sum_{j=1}^M \widehat{\tilde{\pi}}(\mathbf{A}_j)} \leq \frac{\sum_{j=1}^i \widehat{\tilde{\pi}}(\mathbf{A}_j)}{\sum_{j=1}^{\infty} \widehat{\tilde{\pi}}(\mathbf{A}_j)} \leq (1 + \epsilon) \frac{\sum_{j=1}^i \widehat{\tilde{\pi}}(\mathbf{A}_j)}{\sum_{j=1}^M \widehat{\tilde{\pi}}(\mathbf{A}_j)}. \quad (13)$$

Due to (12) and (13), for sufficiently small $\epsilon > 0$, in all practical implementations (10) holds if and only if

$$\frac{\sum_{j=1}^{i-1} \widehat{\tilde{\pi}}(\mathbf{A}_j)}{\sum_{j=1}^M \widehat{\tilde{\pi}}(\mathbf{A}_j)} < U < \frac{\sum_{j=1}^i \widehat{\tilde{\pi}}(\mathbf{A}_j)}{\sum_{j=1}^M \widehat{\tilde{\pi}}(\mathbf{A}_j)} \quad (14)$$

holds. If, in any case, $i = M$, then we shall compute $\widehat{\tilde{\pi}}(\mathbf{A}_j)$; $j = M + 1, \dots, 2M$, and re-check (14) for the same set of uniform random numbers $U \sim U(0, 1)$ as before by replacing M with $2M$, and continue the procedure until all the indices i are less than M .

Once π_i is selected by the above strategy, we can proceed to sample perfectly from π_i . We progress towards building an effective perfect sampling strategy by first establishing a minorization condition for the Markov transition kernel.

3.1 Minorization for π_i

For π_i , we consider the Metropolis-Hastings algorithm in which all the co-ordinates θ_k ; $k = 1, \dots, d$, are updated in a single block using an independence uniform proposal density on \mathbf{A}_i given by

$$q_i(\boldsymbol{\theta}') = \frac{1}{\mathcal{L}(\mathbf{A}_i)} I_{\mathbf{A}_i}(\boldsymbol{\theta}'). \quad (15)$$

Although independence proposal distributions are usually not recommended, particularly in high dimensions, here this makes good sense. Indeed, since \mathbf{A}_i are so constructed that the densities π_i are expected to be relatively flat on these sets, the uniform proposal is expected to provide good approximation to the target π_i . Furthermore, as we shall show, the uniform proposal will be responsible for obtaining significantly large lower bound for our minorization, which, in turn, will play the defining role in our construction of an efficient perfect sampler for π_i .

For $\boldsymbol{\theta} \in \mathbf{A}_i$, for any Borel set \mathbb{B} in the Borel σ -field of \mathbb{R}^d , let $P_i(\boldsymbol{\theta}, \mathbb{B} \cap \mathbf{A}_i)$ denote the corresponding Metropolis-Hastings transition probability for π_i . Let $s_i = \inf_{\boldsymbol{\theta} \in \mathbf{A}_i} \tilde{\pi}(\boldsymbol{\theta})$ and $S_i = \sup_{\boldsymbol{\theta} \in \mathbf{A}_i} \tilde{\pi}(\boldsymbol{\theta})$. Then, with (15) as the proposal density we have

$$\begin{aligned} P_i(\boldsymbol{\theta}, \mathbb{B} \cap \mathbf{A}_i) &\geq \int_{\mathbb{B} \cap \mathbf{A}_i} \min \left\{ 1, \frac{\tilde{\pi}(\boldsymbol{\theta}')}{\tilde{\pi}(\boldsymbol{\theta})} \right\} q_i(\boldsymbol{\theta}') d\boldsymbol{\theta}' \\ &\geq \left(\frac{s_i}{S_i} \right) \times \frac{\mathcal{L}(\mathbb{B} \cap \mathbf{A}_i)}{\mathcal{L}(\mathbf{A}_i)} \\ &= p_i Q_i(\mathbb{B} \cap \mathbf{A}_i), \end{aligned} \quad (16)$$

where $p_i = s_i/S_i$ and

$$Q_i(\mathbb{B} \cap \mathbf{A}_i) = \frac{\mathcal{L}(\mathbb{B} \cap \mathbf{A}_i)}{\mathcal{L}(\mathbf{A}_i)}$$

is the uniform probability measure corresponding to (15). Since (16) holds for all $\boldsymbol{\theta} \in \mathbf{A}_i$, the entire set \mathbf{A}_i is a small set.

Here are some important remarks regarding justification of the choice of the uniform proposal density. First, since the uniform proposal is the independence sampler, independent of the previous state of the underlying Markov chain, the right hand side of (16) is rendered independent of $\boldsymbol{\theta}$, which is a requisite condition for minorization. For proposal distributions of the form $q_i(\boldsymbol{\theta}'|\boldsymbol{\theta})$, infimum of $q_i(\boldsymbol{\theta}'|\boldsymbol{\theta})$ for $\boldsymbol{\theta}, \boldsymbol{\theta}' \in \mathbf{A}_i$ would be necessary, which would lead to much smaller lower bound for $P_i(\boldsymbol{\theta}, \mathbb{B} \cap \mathbf{A}_i)$ compared to the right hand side of (16). This is precisely the reason why we do not consider TMCMC for *iid* sampling, whose move types depend upon the previous state. Any independence proposal density other than the uniform will not get cancelled in the Metropolis-Hastings acceptance ratio and the corresponding s_i/S_i may be vanishingly small if $\tilde{\pi}$ is not well-approximated by the independence proposal on \mathbf{A}_i . This would make perfect sampling infeasible. Furthermore, as will be seen in Section 3.2, for perfect sampling it is required to simulate from the proposal density. But unlike the case of uniform proposal, it may be difficult to simulate from the proposal on \mathbf{A}_i , which has closed ellipsoidal or closed annulus structure.

Observe that s_i and S_i associated with (16) will usually not be available in closed forms. In this regard, let \hat{s}_i and \hat{S}_i denote the minimum and maximum of $\tilde{\pi}(\cdot)$ over the Monte Carlo samples drawn uniformly from \mathbf{A}_i in course of estimating $\tilde{\pi}(\mathbf{A}_i)$ by $\widehat{\tilde{\pi}(\mathbf{A}_i)}$.

Then $\frac{s_i}{S_i} \leq \frac{\hat{s}_i}{\hat{S}_i}$. Hence, there exists $\eta_i > 0$ such that $1 \geq \frac{s_i}{S_i} \geq \frac{\hat{s}_i}{\hat{S}_i} - \eta_i > 0$. Let $\hat{p}_i = \frac{\hat{s}_i}{\hat{S}_i} - \eta_i$. Then it follows from (16) that

$$P_i(\boldsymbol{\theta}, \mathbb{B} \cap \mathbf{A}_i \geq \hat{p}_i) Q_i(\mathbb{B} \cap \mathbf{A}_i), \quad (17)$$

which we shall consider for our purpose from now on. In practice, η_i is expected to be very close to zero, since the Monte Carlo sample size would be sufficiently large. Thus, \hat{p}_i is expected to be very close to p_i .

3.2 Split chain

Due to the minorization (17), $P_i(\boldsymbol{\theta}, \mathbb{B} \cap \mathbf{A}_i)$ admits the following decomposition for all $\boldsymbol{\theta} \in \mathbf{A}_i$:

$$P_i(\boldsymbol{\theta}, \mathbb{B} \cap \mathbf{A}_i) = \hat{p}_i Q_i(\mathbb{B} \cap \mathbf{A}_i) + (1 - \hat{p}_i) R_i(\boldsymbol{\theta}, \mathbb{B} \cap \mathbf{A}_i), \quad (18)$$

where

$$R_i(\boldsymbol{\theta}, \mathbb{B} \cap \mathbf{A}_i) = \frac{P_i(\boldsymbol{\theta}, \mathbb{B} \cap \mathbf{A}_i) - \hat{p}_i Q_i(\mathbb{B} \cap \mathbf{A}_i)}{1 - \hat{p}_i} \quad (19)$$

is the residual distribution.

Therefore, to implement the Markov chain $P_i(\boldsymbol{\theta}, \mathbb{B} \cap \mathbf{A}_i)$, rather than proceeding directly with the uniform proposal based Metropolis-Hastings algorithm, we can use the split (18) to generate realizations from $P_i(\boldsymbol{\theta}, \mathbb{B} \cap \mathbf{A}_i)$. That is, given $\boldsymbol{\theta}$, we can simulate from Q_i with probability \hat{p}_i , and with the remaining probability, can generate from $R_i(\boldsymbol{\theta}, \cdot)$.

To simulate from the residual density $R_i(\boldsymbol{\theta}, \cdot)$ we devise the following rejection sampling scheme. Let $\tilde{R}_i(\boldsymbol{\theta}, \boldsymbol{\theta}')$ and $\tilde{P}_i(\boldsymbol{\theta}, \boldsymbol{\theta}')$ denote the densities of $\boldsymbol{\theta}'$ with respect to $R_i(\boldsymbol{\theta}, \cdot)$ and $P_i(\boldsymbol{\theta}, \cdot)$, respectively. Then it follows from (18) and (19) that for all $\boldsymbol{\theta} \in \mathbf{A}_i$,

$$\begin{aligned} \tilde{R}_i(\boldsymbol{\theta}, \boldsymbol{\theta}') &= \frac{\tilde{P}_i(\boldsymbol{\theta}, \boldsymbol{\theta}') - \hat{p}_i q_i(\boldsymbol{\theta}')}{1 - \hat{p}_i} \leq \frac{\tilde{P}_i(\boldsymbol{\theta}, \boldsymbol{\theta}')}{1 - \hat{p}_i} \\ &\Leftrightarrow \frac{\tilde{R}_i(\boldsymbol{\theta}, \boldsymbol{\theta}')}{\tilde{P}_i(\boldsymbol{\theta}, \boldsymbol{\theta}')} \leq \frac{1}{1 - \hat{p}_i}, \text{ for all } \boldsymbol{\theta}' \in \mathbf{A}_i. \end{aligned}$$

Hence, given $\boldsymbol{\theta}$ we can continue to simulate $\boldsymbol{\theta}' \sim \tilde{P}_i(\boldsymbol{\theta}, \cdot)$ using the uniform proposal distribution (15) and generate $U \sim U(0, 1)$ until

$$U < \frac{(1 - \hat{p}_i)\tilde{R}_i(\boldsymbol{\theta}, \boldsymbol{\theta}')}{\tilde{P}_i(\boldsymbol{\theta}, \boldsymbol{\theta}')} \quad (20)$$

is satisfied, at which point we accept $\boldsymbol{\theta}'$ as a realization from $\tilde{R}_i(\boldsymbol{\theta}, \cdot)$.

Now

$$\begin{aligned} \tilde{P}_i(\boldsymbol{\theta}, \boldsymbol{\theta}') &= q_i(\boldsymbol{\theta}') \min \left\{ 1, \frac{\pi(\boldsymbol{\theta}')}{\pi(\boldsymbol{\theta})} \right\} + r_i(\boldsymbol{\theta}) I_{\boldsymbol{\theta}}(\boldsymbol{\theta}') \\ &= \frac{1}{\mathcal{L}(\mathbf{A}_i)} \min \left\{ 1, \frac{\pi(\boldsymbol{\theta}')}{\pi(\boldsymbol{\theta})} \right\} + r_i(\boldsymbol{\theta}) I_{\boldsymbol{\theta}}(\boldsymbol{\theta}'), \end{aligned}$$

where

$$\begin{aligned} r_i(\boldsymbol{\theta}) &= 1 - \int_{\mathbf{A}_i} \min \left\{ 1, \frac{\pi(\tilde{\boldsymbol{\theta}})}{\pi(\boldsymbol{\theta})} \right\} q_i(\tilde{\boldsymbol{\theta}}) d\tilde{\boldsymbol{\theta}} \\ &= 1 - \int_{\mathbf{A}_i} \min \left\{ 1, \frac{\pi(\tilde{\boldsymbol{\theta}})}{\pi(\boldsymbol{\theta})} \right\} \frac{1}{\mathcal{L}(\mathbf{A}_i)} d\tilde{\boldsymbol{\theta}}. \end{aligned} \quad (21)$$

Let $\hat{r}_i(\boldsymbol{\theta})$ denote the Monte Carlo estimate of $r_i(\boldsymbol{\theta})$ obtained by simulating $\tilde{\boldsymbol{\theta}}$ from the uniform distribution on \mathbf{A}_i and taking the average of $\min \left\{ 1, \frac{\pi(\tilde{\boldsymbol{\theta}})}{\pi(\boldsymbol{\theta})} \right\}$ in (21). Let

$$\begin{aligned} \hat{P}_i(\boldsymbol{\theta}, \boldsymbol{\theta}') &= \frac{1}{\mathcal{L}(\mathbf{A}_i)} \min \left\{ 1, \frac{\pi(\boldsymbol{\theta}')}{\pi(\boldsymbol{\theta})} \right\} + \hat{r}_i(\boldsymbol{\theta}) I_{\boldsymbol{\theta}}(\boldsymbol{\theta}'), \text{ and} \\ \hat{R}_i(\boldsymbol{\theta}, \boldsymbol{\theta}') &= \frac{\hat{P}_i(\boldsymbol{\theta}, \boldsymbol{\theta}') - \hat{p}_i q_i(\boldsymbol{\theta}')}{1 - \hat{p}_i}. \end{aligned}$$

Given $\boldsymbol{\theta}$ and any $\epsilon > 0$, let the Monte Carlo sample size be large enough such that

$$\begin{aligned} 1 - \epsilon &\leq \frac{\tilde{P}_i(\boldsymbol{\theta}, \boldsymbol{\theta}')}{\hat{P}_i(\boldsymbol{\theta}, \boldsymbol{\theta}')} \leq 1 + \epsilon, \text{ and} \\ 1 - \epsilon &\leq \frac{\tilde{R}_i(\boldsymbol{\theta}, \boldsymbol{\theta}')}{\hat{R}_i(\boldsymbol{\theta}, \boldsymbol{\theta}')} \leq 1 + \epsilon. \end{aligned}$$

Then

$$\left(\frac{1 - \epsilon}{1 + \epsilon} \right) \frac{\tilde{R}_i(\boldsymbol{\theta}, \boldsymbol{\theta}')}{\tilde{P}_i(\boldsymbol{\theta}, \boldsymbol{\theta}')} \leq \frac{\hat{R}_i(\boldsymbol{\theta}, \boldsymbol{\theta}')}{\hat{P}_i(\boldsymbol{\theta}, \boldsymbol{\theta}')} \leq \left(\frac{1 + \epsilon}{1 - \epsilon} \right) \frac{\tilde{R}_i(\boldsymbol{\theta}, \boldsymbol{\theta}')}{\tilde{P}_i(\boldsymbol{\theta}, \boldsymbol{\theta}')} \quad (22)$$

Due to (22), in all practical implementations, for sufficiently small $\epsilon > 0$, (20) holds if and only if

$$U < \frac{(1 - \hat{p}_i) \hat{R}_i(\boldsymbol{\theta}, \boldsymbol{\theta}')}{\hat{P}_i(\boldsymbol{\theta}, \boldsymbol{\theta}')} \quad (23)$$

holds. Hence, we shall carry out our implementations with (23).

3.3 Perfect simulation from π_i

For perfect simulation we exploit the following idea first presented in [Murdoch and Green \(1998\)](#). From (18) note that at any given positive time $T_i = t$, $\boldsymbol{\theta}'$ will be drawn from $Q_i(\cdot)$ with probability \hat{p}_i . Also observe that T_i can not take the value 0, since only initialization is done at the zero-th time point. Hence, T_i follows a geometric distribution given by

$$P(T_i = t) = \hat{p}_i (1 - \hat{p}_i)^{t-1}; \quad t = 1, 2, \dots \quad (24)$$

This is in contrast with the form of the geometric distribution provided in [Murdoch and Green \(1998\)](#), which gives positive probability to $T_i = 0$ (in our context, $P(T_i = t) = \hat{p}_i (1 - \hat{p}_i)^t$; $t = 0, 1, 2, \dots$, with respect to their specification). Indeed, all our implementations yielded correct *iid* simulations only for the form (24) and failed to provide correct answers for that of [Murdoch and Green \(1998\)](#).

Because of (24), it is possible to simulate T_i from the geometric distribution and then draw $\boldsymbol{\theta}^{(-T_i)} \sim Q_i(\cdot)$. Then the chain only needs to be carried forward in time till

$t = 0$, using $\boldsymbol{\theta}^{(t+1)} = \psi_i(\boldsymbol{\theta}^{(t)}, \mathbf{U}_i^{(t+1)})$, where $\psi_i(\boldsymbol{\theta}^{(t)}, \mathbf{U}_i^{(t+1)})$ is the deterministic function corresponding to the simulation of $\boldsymbol{\theta}^{(t+1)}$ from $\tilde{R}_i(\boldsymbol{\theta}^{(t)}, \cdot)$ using the set of appropriate random numbers $\mathbf{U}_i^{(t+1)}$; the sequence $\{\mathbf{U}_i^{(t)}; t = 0, -1, -2, \dots\}$ being assumed to be available before beginning the perfect sampling implementation. The resulting draw $\boldsymbol{\theta}^{(0)}$ sampled at time $t = 0$ is a perfect sample from $\pi_i(\cdot)$.

In practice, storing the uniform random numbers $\{\mathbf{U}_i^{(t)}; t = 0, -1, -2, \dots\}$ or explicitly considering the deterministic relationship $\boldsymbol{\theta}^{(t+1)} = \psi_i(\boldsymbol{\theta}^{(t)}, \mathbf{U}_i^{(t+1)})$, are not required. These would be required only if we had taken the search approach, namely, iteratively starting the Markov chain at all initial values at negative times and carrying the sample paths to zero.

4 The complete algorithm for *iid* sample generation from π

We present the complete algorithm for generating *iid* realizations from the target distribution π as Algorithm 1.

Algorithm 1. *IID sampling from the target distribution π*

- (1) Using TCMC based estimates, obtain $\boldsymbol{\mu}$ and $\boldsymbol{\Sigma}$ required for the sets \mathbf{A}_i ; $i \geq 1$.
- (2) Fix M to be sufficiently large.
- (3) Choose the radii $\sqrt{c_i}$; $i = 1, \dots, M$ appropriately. A general strategy for these selections will be discussed in the context of the applications.
- (4) Compute the Monte Carlo estimates $\widehat{\pi}(\mathbf{A}_i)$; $i = 1, \dots, M$, in parallel processors. Thus, M parallel processors will obtain all the estimates simultaneously.
- (5) Instruct each processor to send its respective estimate to all the other processors.
- (6) Let K be the required *iid* sample size from the target distribution π . Split the job of obtaining K *iid* realizations into parallel processors, each processor scheduled to simulate a single realization at a time. That is, with K parallel processors, K realizations will be simulated simultaneously. In each processor, do the following:
 - (i) Select π_i with probability proportional to $\widehat{\pi}(\mathbf{A}_i)$.
 - (ii) If $i = M$ for any processor, then return to Step (2), increase M to $2M$, and repeat the subsequent steps (in Step (4) only $\widehat{\pi}(\mathbf{A}_i)$; $i = M + 1, \dots, 2M$, need to be computed). Else
 - (a) Draw $T_i \sim \text{Geometric}(\hat{p}_i)$ with respect to (24).
 - (b) Draw $\boldsymbol{\theta}^{(-T_i)} \sim Q_i(\cdot)$.
 - (c) Using $\boldsymbol{\theta}^{(-T_i)}$ as the initial value, carry the chain $\boldsymbol{\theta}^{(t+1)} \sim \tilde{R}_i(\boldsymbol{\theta}^{(t)}, \cdot)$ forward for $t = -T_i, -T_i + 1, \dots, -1$.

- (d) From the current processor, send $\theta^{(0)}$ to processor 0 as a perfect realization from π .
- (7) Processor 0 stores the K *iid* realizations $\{\theta_1^{(0)}, \dots, \theta_K^{(0)}\}$ thus generated from the target distribution π .
-

Figures 1–3 provide a schematic illustration of the proposed methodology for generating *iid* samples from an arbitrary target distribution $\pi(\theta)$.

Figure 1 presents the conceptual overview of the *iid* sampling algorithm. The target distribution is decomposed into a sequence of concentric ellipsoidal or annular regions $\{\mathbf{A}_i\}$, each associated with probability $\pi(\mathbf{A}_i)$. A component distribution $\pi_i(\theta)$ is selected with probability proportional to $\pi(\mathbf{A}_i)$, and a perfect sample is drawn from it. Repeating this procedure yields *iid* realizations from the full target $\pi(\theta)$.

Figure 2 illustrates the perfect sampling mechanism within a chosen component \mathbf{A}_i . The Metropolis–Hastings transition kernel P_i is expressed through the minorization inequality $P_i \geq \hat{p}_i Q_i$, leading to $P_i = \hat{p}_i Q_i + (1 - \hat{p}_i) R_i$, where Q_i denotes the uniform distribution over \mathbf{A}_i and R_i represents the residual. This allows a split-chain representation in which a random coalescence time T_i is drawn from a geometric distribution, and the chain is propagated forward to obtain a perfect draw $\theta^{(0)} \sim \pi_i$.

Figure 3 depicts the parallel implementation architecture of the algorithm. Each worker processor estimates its corresponding component weight $\hat{\pi}(\mathbf{A}_i)$ and performs perfect sampling independently. The master processor aggregates all draws $\{\theta_1, \dots, \theta_K\}$ to form a collection of *iid* samples from the overall target distribution $\pi(\theta)$.

5 Experiments with standard distributions

To illustrate our *iid* sampling methodology, we now apply the same to generate *iid* samples from standard distributions, namely, normal, Student’s t (with 5 degrees of freedom), Cauchy, and mixture of normals. We consider both univariate and multivariate versions of the distributions, with dimensions $d = 1, 5, 10, 50, 100$. For the location vector, we set $\nu = (\nu_1, \dots, \nu_d)^T$, with $\nu_i = i$, for $i = 1, \dots, d$. We denote the $d \times d$ scale matrix by \mathbf{S} , whose (i, j) -th element is specified by $S_{ij} = 10 \times \exp\{-(i - j)^2/2\}$. We also consider a mixture of two normals for $d = 50$ with the means being $\nu_1 = \nu$ and $\nu_2 = 2\nu$, and the covariance matrix \mathbf{S} the same as the above for both the normal components. The mixing proportions of the normals associated with ν_1 and ν_2 are $2/3$ and $1/3$, respectively. For illustrative purposes, we assume that $\mu = \nu$ and $\Sigma = \mathbf{S}$ associated with the sets \mathbf{A}_i . In the normal mixture setup, there are two relevant sets of the form \mathbf{A}_i for each i , associated with the two mixture components. We denote these sets by \mathbf{A}_{1i} and \mathbf{A}_{2i} , associated with $\mu = \nu_1$ and $\mu = \nu_2$, respectively, while $\Sigma = \mathbf{S}$ in both the cases. In \hat{p}_i , we set $\eta_i = 10^{-5}$ in all the simulation experiments.

Details of our *iid* simulation procedure and the results for the different standard distributions are presented below. All our codes are written in C using the Message Passing Interface (MPI) protocol for parallel processing. We implemented our codes on a 80-core VMWare provided by Indian Statistical Institute. The machine has 2 TB memory and each core has about 2.8 GHz CPU speed.

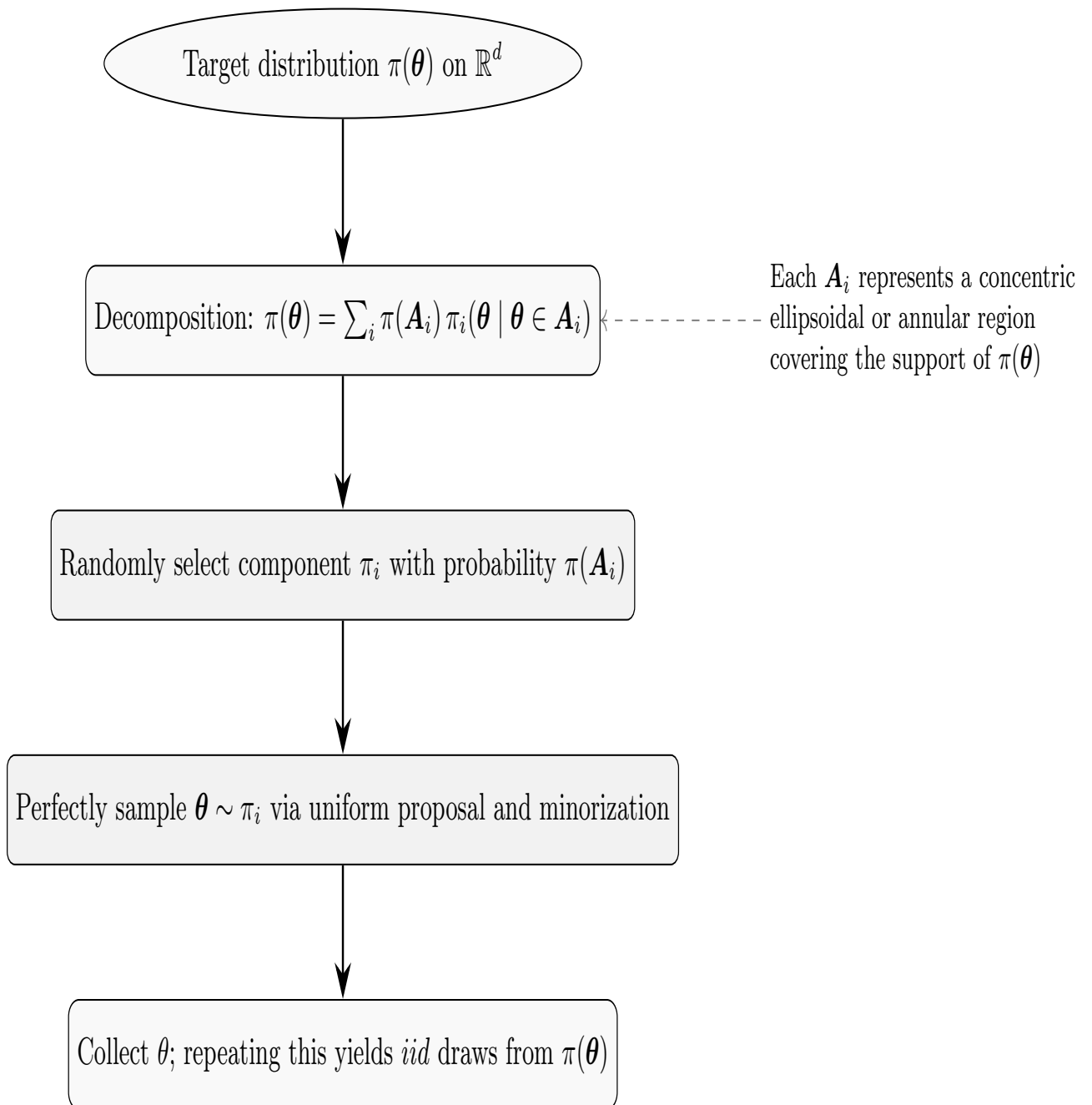


Figure 1: Schematic diagram: the conceptual overview.

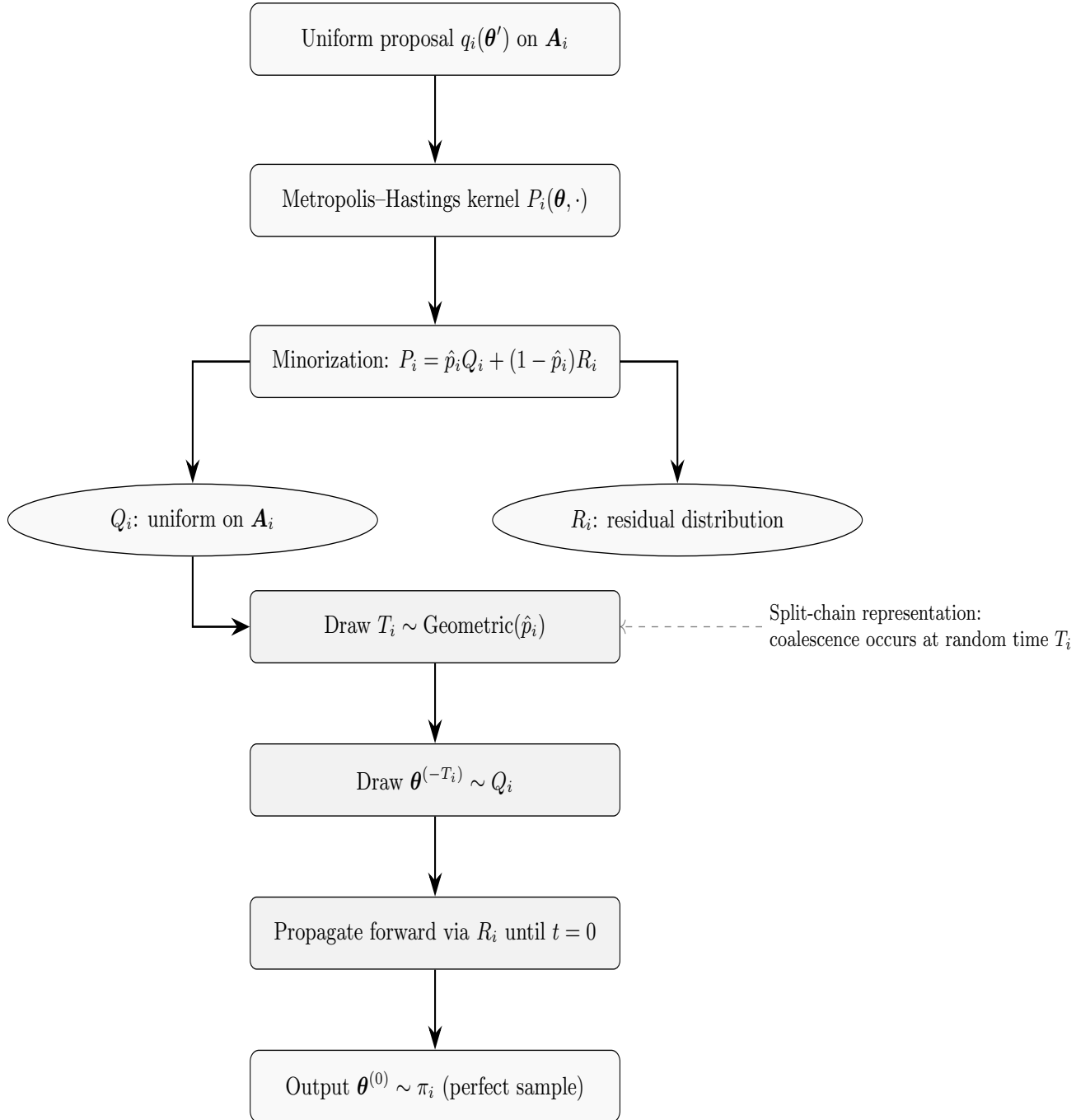
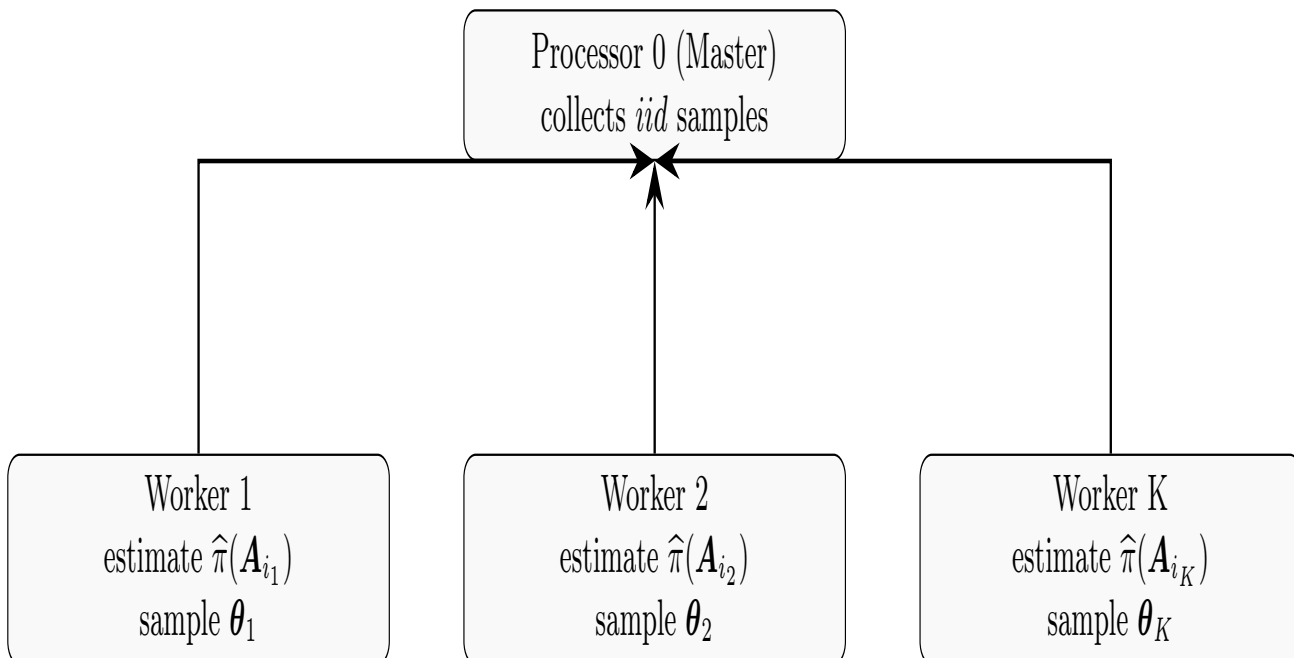


Figure 2: Schematic diagram: perfect sampling.



Each worker independently:
 (1) Monte Carlo estimate of $\hat{\pi}(\mathbf{A}_{i_j})$; $i_j \in \{1, \dots, M\}$; (2) compute $\hat{p}_i, \hat{P}_i, \hat{R}_i$; (3) draw $T_i, \boldsymbol{\theta}^{(-T_i)}$; (4) propagate $\rightarrow \boldsymbol{\theta}^{(0)}$.
 Master aggregates $\{\boldsymbol{\theta}_1, \dots, \boldsymbol{\theta}_K\}$ to form *iid* sample set.

Figure 3: Schematic diagram: parallel implementation.

5.1 Simulation from normals

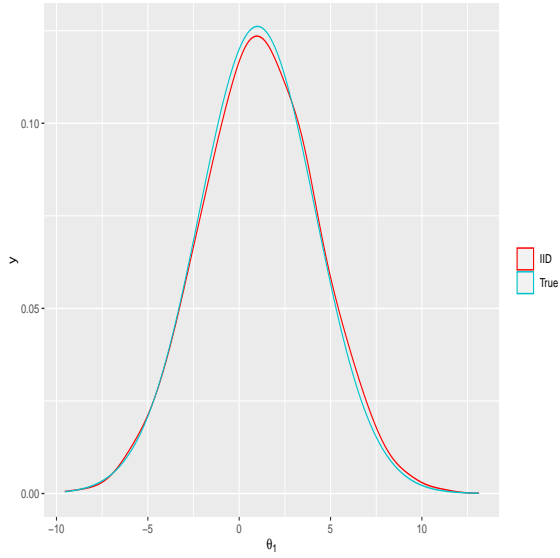
For $d = 1, 5, 10, 50, 100$, we set $\sqrt{c_1} = 4$ and for $i = 2, \dots, M$, set $\sqrt{c_i} = \sqrt{c_1} + (i - 1)/2$. With these choices of the radii, it turned out that $M = 71$ was sufficient for all the dimensions considered. The choice of such forms of the radii has been guided by the insight that the target distribution is concentrated on \mathbf{A}_1 , and the sets \mathbf{A}_i , for increasing i , encapsulate the tail regions. Thus, setting $\sqrt{c_1}$ somewhat large and keeping the difference $\sqrt{c_i} - \sqrt{c_{i-1}}$ adequately small for $i > 1$, seems to be a sensible strategy for giving more weight to the modal region and less weight to the tail regions. Of course, it has to be borne in mind that a larger value of $\sqrt{c_1}$ than what is adequate can make \hat{p}_1 extremely small, since for larger radii s_1 would be smaller and S_1 larger (see (16)). The explicit choices in our cases are based on experimentations after fixing the forms of the radii for dimension d as follows: $\sqrt{c_1} = r_d$ and for $i = 2, \dots, M$, $\sqrt{c_i} = \sqrt{c_1} + a_d \times (i - 1)$. The values of M , r_d and a_d that yielded sufficiently large values of \hat{p}_i ; $i = 1, \dots, M$, for Monte Carlo size $N_i = 10,000$, are considered for our applications. With a given choice of M , if \mathbf{A}_M is represented in the set of *iid* realizations, then we increase M to $2M$ and repeat the experiment, as suggested in Section 3 and made explicit in Algorithm 1. This basic method of selecting the radii and M will remain the same in all our applications.

With the Monte Carlo size $N_i = 10,000$ used for the construction of $\hat{\pi}(\boldsymbol{\theta})$, we then simulated 10,000 *iid* realizations from $\hat{\pi}(\boldsymbol{\theta})$, which took 57 minutes, 1 hour 45 minutes, 25 minutes, 6 minutes, and 1 hour 39 minutes on our VMWare, for $d = 1, 5, 10, 50, 100$, respectively. In all the cases, the true marginal densities and the correlation structures are very accurately captured by the *iid* samples generated by our methodology. For the sake of brevity, we display in Figure 4 the results for only four co-ordinates in the context of $d = 100$. The exact and estimated correlation structures for the first 20 co-ordinates are displayed in Figure 5.

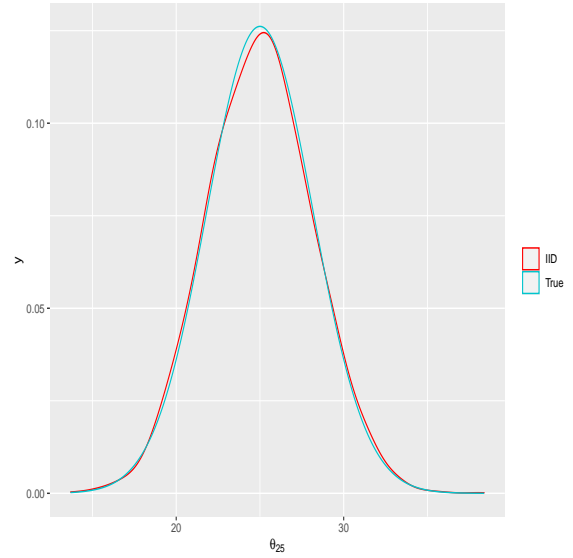
5.2 Simulation from Student's t with 5 degrees of freedom

In the Student's t setup, $M = 1000$ turned out to be sufficient for all the dimensions that we considered; this significantly larger value of M compared to that for the normal setup is due to the much thicker tails of the t distribution with 5 degrees of freedom. Depending upon the dimension, we chose the radii differently for adequate performance of our methodology. The general form of our choice is the same as in the normal setup, that is, $\sqrt{c_1} = r_d$ and $\sqrt{c_i} = \sqrt{c_1} + a_d \times (i - 1)$, for $i = 2, \dots, M$. Following our experimentations as discussed in the normal simulation context, we set $r_1 = 5$ and $r_d = 4$, for $d = 5, 10, 50, 100$. As regards a_d , we set $a_1 = 3.801$, $a_5 = 2.1654$, $a_{10} = 2.5$, $a_{50} = 0.52$ and $a_{100} = 0.52$. As before, we used Monte Carlo size $N_i = 10,000$ for the construction of $\hat{\pi}(\boldsymbol{\theta})$, and then simulated 10,000 *iid* realizations from $\hat{\pi}(\boldsymbol{\theta})$. The times taken for $d = 1, 5, 10, 50, 100$ are 4 minutes, 29 minutes, 1 hour 3 minutes, less than a minute, and less than a minute, respectively. The reason for the significantly less time here compared to the normal setup is again attributable to the thick tails of the t distribution; the flatter tails ensure that the infimum s_i and supremum S_i are not much different, entailing that \hat{p}_i is reasonably large (see (16)), so that simulation from the geometric distribution (24) yielded significantly smaller values of the coalescence time T_i compared to the normal setup. Thus, in spite of the larger value of M , these small values of T_i led to much quicker overall computation.

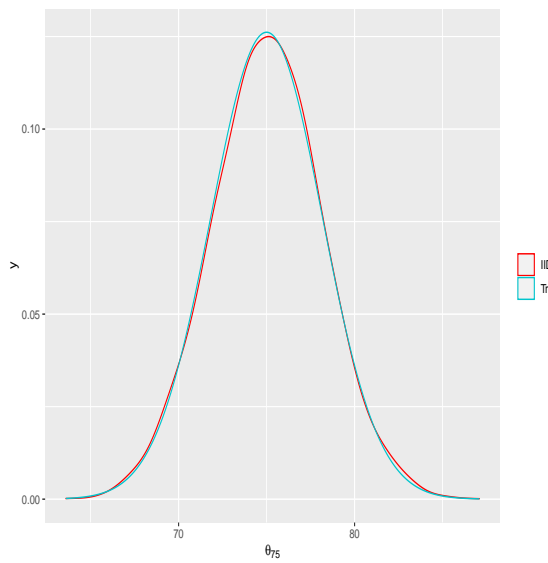
Again, the *iid* simulations turned out to be highly reliable in all the cases. Figure 6 shows the results for four co-ordinates in the context of $d = 100$, and the exact and



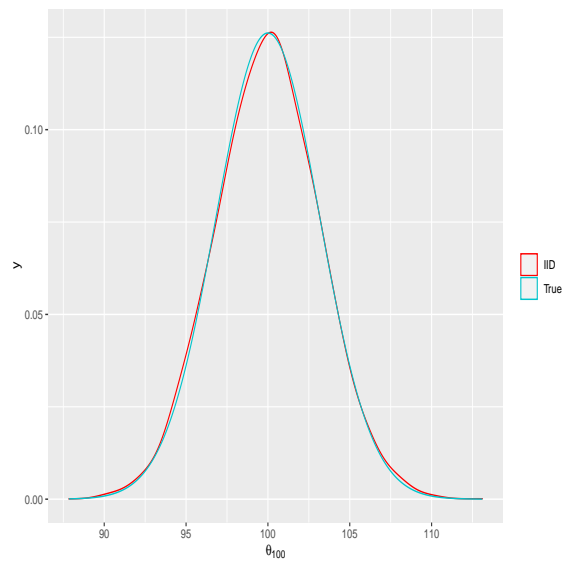
(a) True and *iid*-based density for θ_1 .



(b) True and *iid*-based density for θ_{25} .

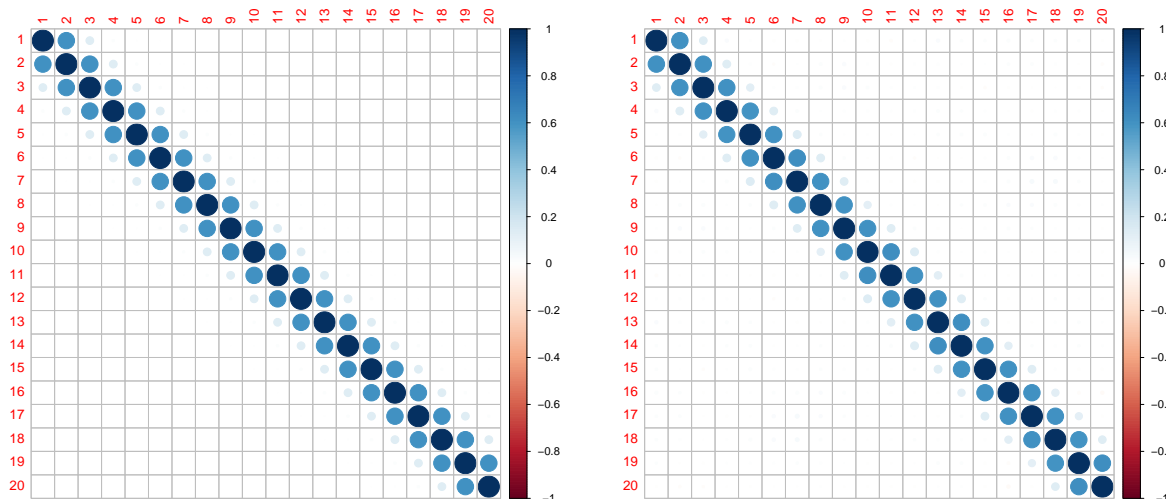


(c) True and *iid*-based density for θ_{75} .



(d) True and *iid*-based density for θ_{100} .

Figure 4: Simulation from 100-dimensional normal distribution. The red and blue colours denote the *iid* sample based density and the true density, respectively.



(a) Exact correlation structure.

(b) Correlation structure based on *iid* samples.

Figure 5: Simulation from 100-dimensional normal distribution. True and *iid*-based correlation structures for the first 20 co-ordinates.

estimated correlation structures for the first 20 co-ordinates are displayed in Figure 7.

5.3 Simulation from Cauchy

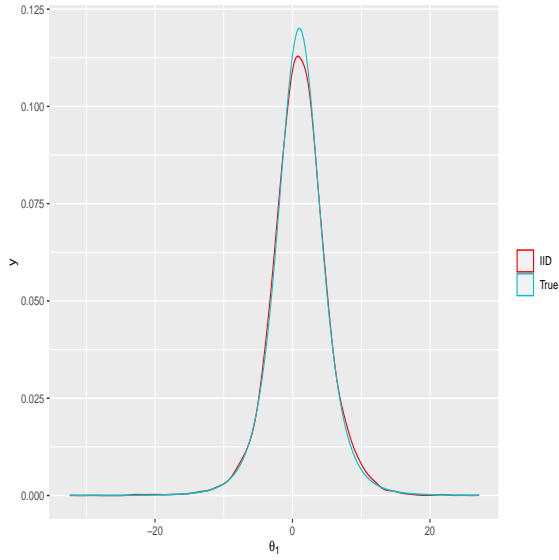
In this case, we set $\sqrt{c_1} = r_d$ and $\sqrt{c_i} = \sqrt{c_1} + a_d \times (i - 1)$, for $i = 2, \dots, M_d$. Thus, even the value of M now depends upon d . Following our experimentations we obtained the following: $(r_1 = 5, a_1 = 3.801, M_1 = 2000)$, $(r_5 = 0.5, a_5 = 0.5, M_5 = 3000)$, $(r_{10} = 0.5, a_{10} = 0.5, M_{10} = 3000)$, $(r_{50} = 4, a_{50} = 0.52, M_{50} = 2000)$, $(r_{100} = 4, a_{100} = 0.52, M_{100} = 2576)$. Note that the values of M_d are at least twice that for the Student's t distribution, which is clearly due to the much thicker tail of Cauchy compared to t .

As before, using Monte Carlo size $N_i = 10,000$ for the construction of $\hat{\pi}(\theta)$, we then simulated 10,000 *iid* realizations from $\hat{\pi}(\theta)$. In this case, the times taken for $d = 1, 5, 10, 50, 100$ are 2 minutes, 2 minutes, 2 minutes, less than a minute, and 2 minutes, respectively. Notice the significantly less time taken in this setup compared to both normal and Cauchy. Given the thickest tail of Cauchy, the reason for this is the same as provided in Section 5.2 that explains lesser time for t compared to normal.

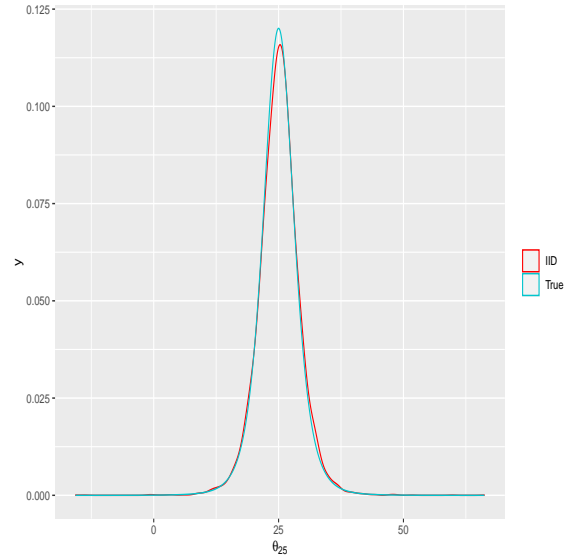
As expected, the *iid* simulations accurately represented the underlying Cauchy distributions. Depictions of the true and *iid* sample based marginal densities of four co-ordinates are presented by Figure 8 in the context of $d = 100$. Since the covariance structure does not exist for Cauchy, we do not present the correlation structure comparison unlike the previous cases.

5.4 Simulation from normal mixture

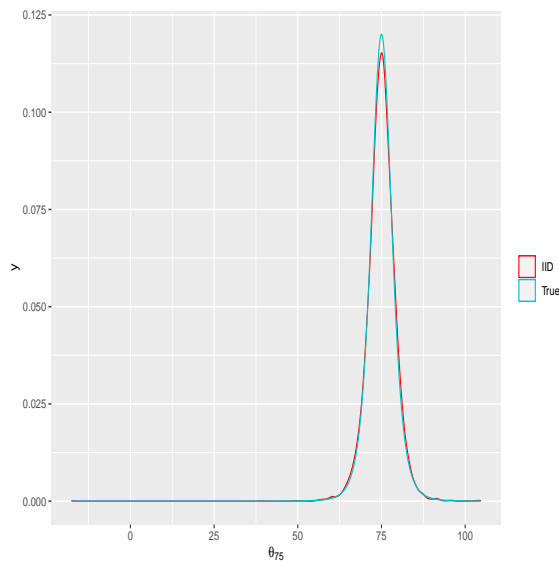
In this case, for both A_{1i} and A_{2i} , we chose $r_{50} = 4$ and $a_{50} = 0.5$. As in the normal setup detailed in Section 5.1, $M = 71$ turned out to be sufficient. We set $N_i = 10,000$



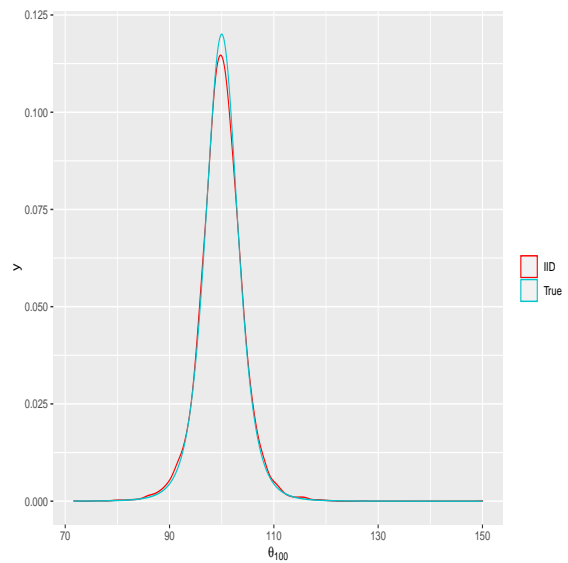
(a) True and *iid*-based density for θ_1 .



(b) True and *iid*-based density for θ_{25} .

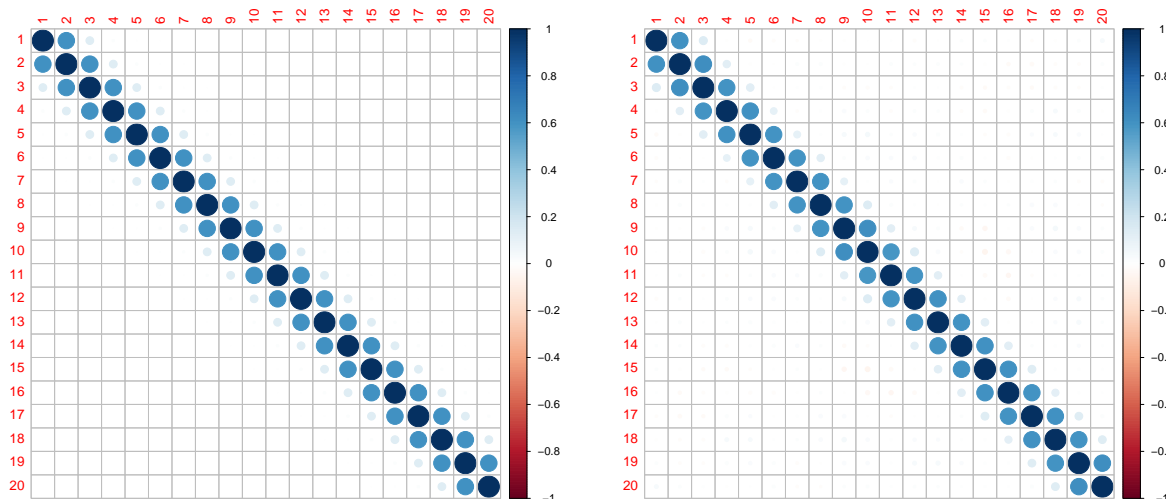


(c) True and *iid*-based density for θ_{75} .



(d) True and *iid*-based density for θ_{100} .

Figure 6: Simulation from 100-dimensional Student's t distribution with 5 degrees of freedom. The red and blue colours denote the *iid* sample based density and the true density, respectively.



(a) Exact correlation structure.

(b) Correlation structure based on *iid* samples.

Figure 7: Simulation from 100-dimensional Student’s t distribution with 5 degrees of freedom. True and *iid*-based correlation structures for the first 20 co-ordinates.

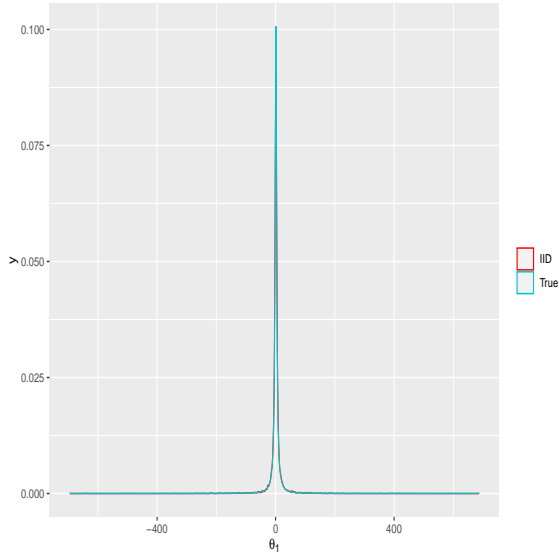
as the Monte Carlo size, as in the previous cases. For drawing each *iid* realization, assuming known mixing probabilities $2/3$ and $1/3$, we first selected either of the two mixing densities, indexed by $j = 1, 2$. Then, with the corresponding sequence of sets \mathbf{A}_{ji} , we proceeded with perfect sampling from the mixing density indexed by j . The time taken for the entire implementation was 7 minutes for generating 10,000 *iid* realizations.

As before, the *iid* realizations very accurately represented the true mixture distribution, Figure 9 bearing some testimony. Figure 10 compares the true correlation structure and that estimated by our *iid* method. As expected, the estimated structure yielded by our *iid* method has been highly accurate. Here it is worth remarking that the true correlation structure is also an estimated structure, based on 10,000 direct *iid* realizations from the normal mixture.

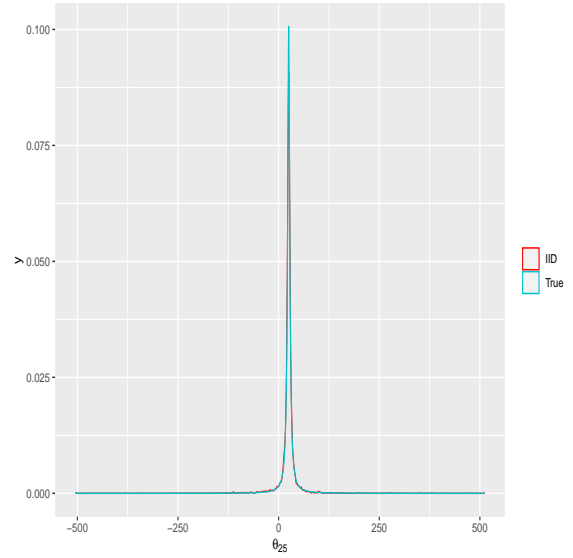
Details of the method for generating perfect *iid* realizations from any general multimodal target distribution π , is provided in [Bhattacharya \(2021b\)](#).

6 Experiments with posterior distributions given real data

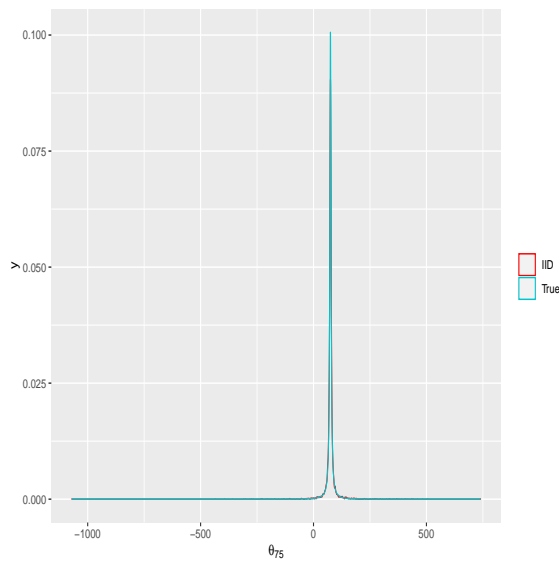
We now consider the application of our *iid* method to posterior distributions given real datasets. Our first application in this regard will be the well-known Challenger space shuttle problem (see, for example, [Dalal et al. \(1989\)](#), [Martz and Zimmer \(1992\)](#), [Robert and Casella \(2004\)](#) and [Dutta and Bhattacharya \(2014\)](#)). The data can be found in [Robert and Casella \(2004\)](#) and in the supplement of [Dutta and Bhattacharya \(2014\)](#). Here we consider drawing *iid* realizations from the two-parameter posterior distribution corresponding to a logit likelihood and compare the *iid* based and TMCMC



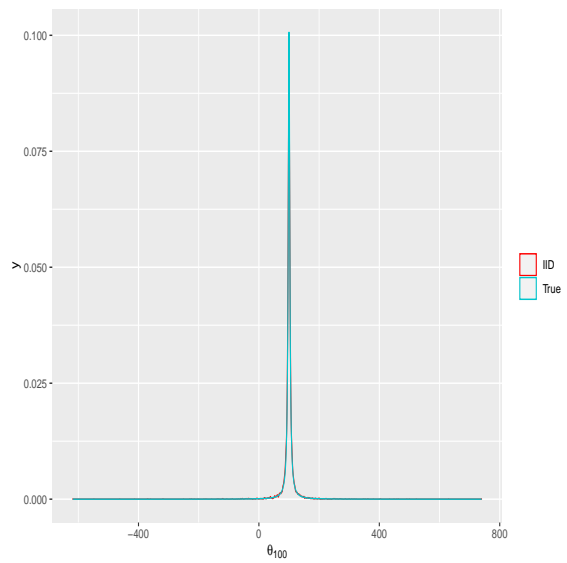
(a) True and *iid*-based density for θ_1 .



(b) True and *iid*-based density for θ_{25} .

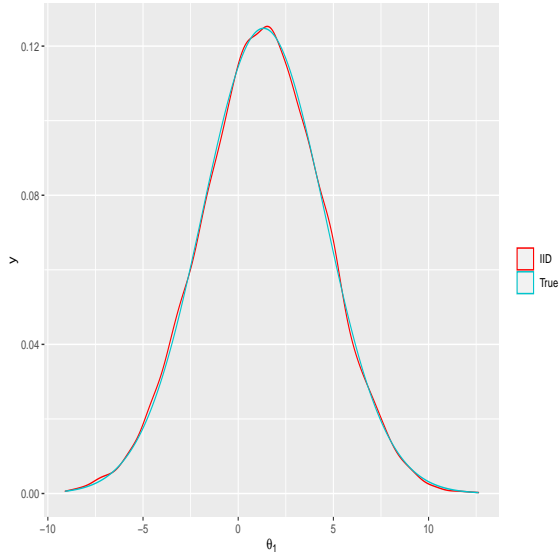


(c) True and *iid*-based density for θ_{75} .

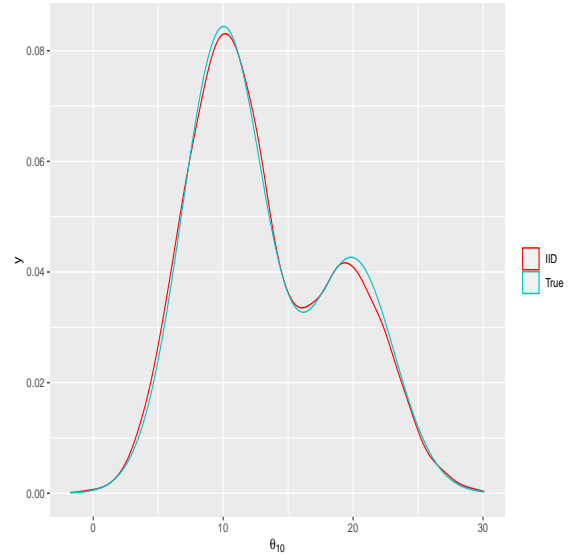


(d) True and *iid*-based density for θ_{100} .

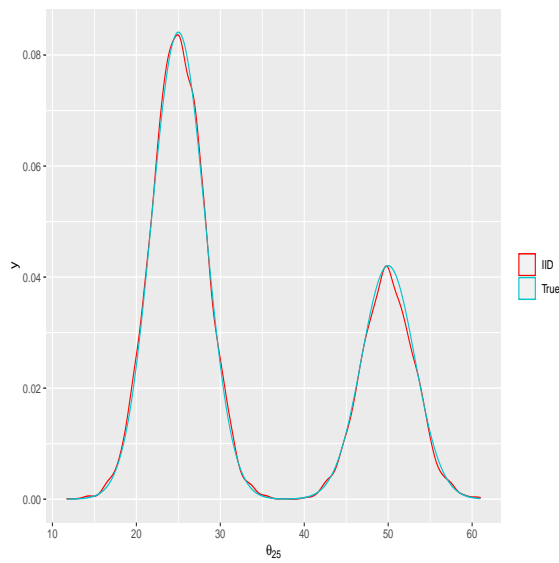
Figure 8: Simulation from 100-dimensional Cauchy distribution. The red and blue colours denote the *iid* sample based density and the true density, respectively.



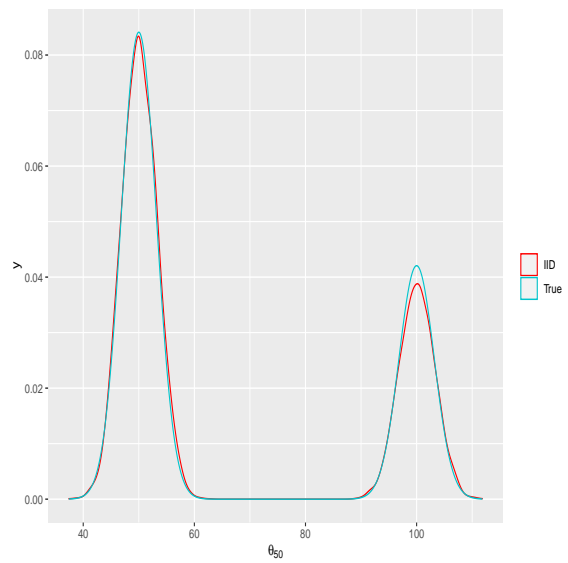
(a) True and *iid*-based density for θ_1 .



(b) True and *iid*-based density for θ_{10} .

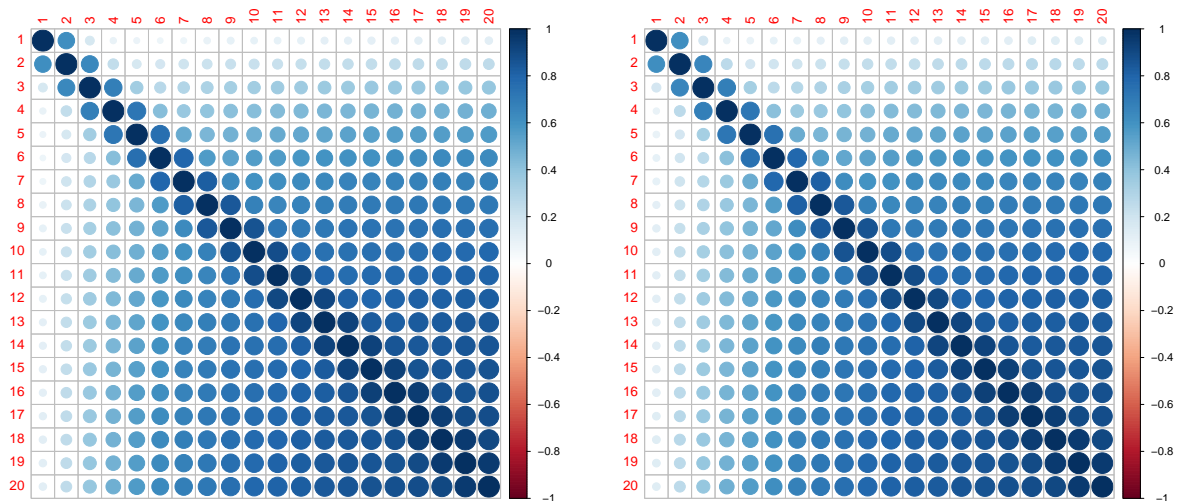


(c) True and *iid*-based density for θ_{25} .



(d) True and *iid*-based density for θ_{50} .

Figure 9: Simulation from 50-dimensional mixture normal distribution. The red and blue colours denote the *iid* sample based density and the true density, respectively.



(a) Exact correlation structure.

(b) Correlation structure based on *iid* samples.

Figure 10: Simulation from 50-dimensional mixture normal distribution. True and *iid*-based correlation structures for the first 20 co-ordinates.

based posteriors.

For our second application, we shall consider the Salmonella example from Chapter 6.5.2 of [Lunn *et al.* \(2012\)](#). The data, three-parameter Poisson log-linear model, the priors and the BUGS/JAGS codes are also available at <http://runjags.sourceforge.net/quickjags.html>. In this example as well, we shall compare the *iid* based and TMCMC based posteriors.

Our third application is on the really challenging, spatial data and model setup related to radionuclide count data on Rongelap Island ([Diggle *et al.* \(1997\)](#), [Diggle *et al.* \(1998\)](#)). The model for the radionuclide counts is a Poisson log-linear model encapsulating a latent Gaussian process to account for spatial dependence. The model consists of 160 parameters. The difficulty of MCMC convergence for the posterior analysis in this problem is very well-known and several research works have been devoted to this (see, for example, [Rue \(2001\)](#), [Christensen \(2004\)](#), [Christensen \(2006\)](#)). Very encouragingly, even in this challenging problem, we are able to very successfully obtain *iid* samples from the posterior, after using a specific diffeomorphic transformation to the posterior to render it sufficiently thick-tailed to yield reasonably large values of \hat{p}_i . As in the previous examples, here also we shall compare the *iid* and TMCMC based posteriors.

6.1 Application to the Challenger dataset

In 1986, the space shuttle Challenger exploded during take off, killing the seven astronauts aboard. The explosion was the result of an O-ring failure, a splitting of a ring of rubber that seals the parts of the ship together. The accident was believed to be caused by the unusually cold weather (31°F or 0°C) at the time of launch, as there is reason to believe that the O-ring failure probabilities increase as temperature decreases.

In this regard, for $i = 1, \dots, n$, where $n = 23$, let y_i denote the indicator variable

denoting failure of the O-ring. Also let $x_i = t_i / \max t_i$, where t_i is the temperature (degrees F) at flight time i . We assume that for $i = 1, \dots, n$, $y_i \sim \text{Bernoulli}(p(x_i))$ independently, where $p(x_i) = \exp(\alpha + \beta x_i) / (1 + \exp(\alpha + \beta x_i))$. As regards the prior for (α, β) , we set $\pi(\alpha, \beta) \equiv 1$ for $\alpha, \beta \in \mathbb{R}$.

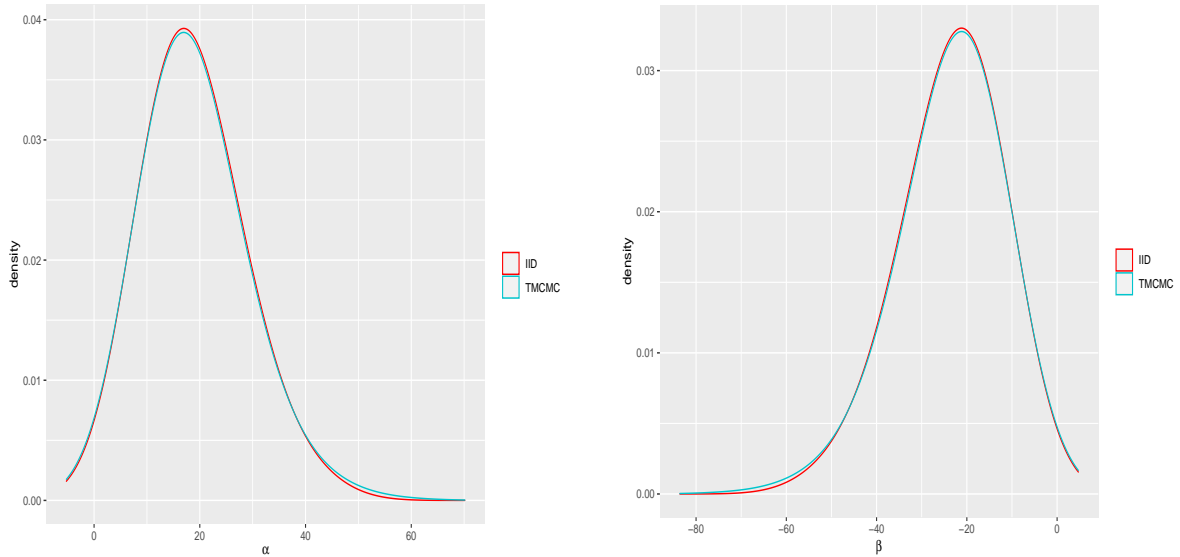
For TMCMC, we consider the additive transformation detailed in Section 4 of [Dutta and Bhattacharya \(2014\)](#), with scaling constants in the additive transformation being 7.944 and 9.762 respectively for α and β . After accepting the proposed additive TMCMC move or the previous state in accordance with the TMCMC acceptance probability, we conduct another mixing-enhancement step in a similar vein as in [Liu and Sabatti \(2000\)](#) which, given the current accepted state, proposes another move that gives either forward transformation to both the parameters or backward transformation to both the parameters, with equal probability. Either this final move, or the last accepted additive TMCMC move is accepted in accordance with the TMCMC acceptance probability. With this strategy, we run our chain for 2×10^5 iterations, discarding the first 10^5 as burn-in. We estimate $\boldsymbol{\mu}$ and $\boldsymbol{\Sigma}$ required for our sets \mathbf{A}_i using the stored 10^5 iterations after burn-in.

In order to select the radii, we set as before, with $d = 2$, $\sqrt{c_1} = r_d$ and $\sqrt{c_i} = \sqrt{c_1} + a_d \times (i - 1)$, for $i = 2, \dots, M$. Our experiments indicated that $M = 85$, $r_d = 2$ and $a_d = 0.02$ are appropriate choices. Now, since $\sqrt{c_2} - \sqrt{c_1} = 2 \times 0.02$ and $\sqrt{c_i} - \sqrt{c_{i-1}} = 0.02$ for $i \geq 3$, rejection sampling in order to simulate uniformly from \mathbf{A}_i for $i \geq 2$ is costly computationally, since the probability of any point $\tilde{\boldsymbol{\theta}}$ drawn uniformly from the ellipsoid $\{\boldsymbol{\theta} : (\boldsymbol{\theta} - \boldsymbol{\mu})^T \boldsymbol{\Sigma}^{-1} (\boldsymbol{\theta} - \boldsymbol{\mu}) \leq c_i\}$ to satisfy $(\tilde{\boldsymbol{\theta}} - \boldsymbol{\mu})^T \boldsymbol{\Sigma}^{-1} (\boldsymbol{\theta} - \tilde{\boldsymbol{\mu}}) > c_{i-1}$, is small. To handle this, we adopt the following strategy. First observe that in this situation, \mathbf{A}_i here is well approximated by the region close to the surface of the above ellipsoid. For sufficiently large value of \tilde{d} , $\tilde{\mathbf{Y}} = \sqrt{c_i} U^{1/\tilde{d}} \mathbf{X} / \|\mathbf{X}\|$ with $\mathbf{X} = (X_1, \dots, X_d)^T$ where $X_k \stackrel{iid}{\sim} N(0, 1)$, for $k = 1, \dots, d$, $U \sim U(0, 1)$, represents the uniform distribution essentially about the surface of the ball centered around $\mathbf{0}$ and with radius $\sqrt{c_i}$, so that $\tilde{\boldsymbol{\theta}} = \boldsymbol{\mu} + \mathbf{B}\tilde{\mathbf{Y}}$ essentially represents the desired uniform distribution on \mathbf{A}_i . Thus, this method completely avoids rejection sampling. Setting $\tilde{d} = 10^5$ turned out to yield quite accurate results with this strategy. Indeed, comparison with actual rejection sampling showed that the final results are almost indistinguishable.

Instead of setting $N_i = 10,000$ as the Monte Carlo size as in our experiments with the standard distributions, here we set $N_i = 5000$. One obvious reason for this is to reduce the computing time, since there are $M = 10^5$ set \mathbf{A}_i where the Monte Carlo method needs to be applied to. Another reason is that, due to the narrow regions covered individually by the current sets \mathbf{A}_i , not much Monte Carlo realizations are necessary. Again, we compared the results with actual rejection sampling by setting $N_i = 10,000$, and again the final results turned out to be almost the same.

There is another subtle issue that deserves mention. The above strategy for avoiding rejection sampling does not guarantee that none of the points sampled from \mathbf{A}_i will fall in \mathbf{A}_{i-1} , for $i \geq 2$. Indeed, a few points must percolate into \mathbf{A}_{i-1} , but are still counted for computation of the infimum and supremum of $\tilde{\pi}(\boldsymbol{\theta})$ in \mathbf{A}_i . These points thus render the effect of lowering the value of the ratio of the actual infimum and supremum. To counter this effect, we set $\eta_i = 0$ in the formula for \hat{p}_i . Note however, that the Monte Carlo estimate of $\tilde{\pi}(\mathbf{A}_i)$ is unaffected by this percolation since the effect of the few points, when divided by the Monte Carlo size, is washed away.

As before, we sampled 10,000 *iid* realizations from this Challenger posterior. The implementation time of our *iid* method has been 22 minutes for this problem.



(a) TCMC and *iid*-based density for α .

(b) TCMC and *iid*-based density for β .

Figure 11: Challenger posterior. The red and blue colours denote the *iid* sample based density and the TCMC based density, respectively.

Figure 11 compares the *iid* based and TCMC based marginal posteriors of α and β . Here we thinned the 10^5 TCMC realizations by using one in every 10 for comparing with our 10,000 *iid* realizations. Observe that the *iid* based densities are in very close agreement with those based on TCMC.

The TCMC and *iid* based posterior correlations between α and β are -0.99771 -0.99761 , respectively, exhibiting close agreement.

6.2 Application to the Salmonella dataset

Here the data concerned is a mutagenicity assay data on Salmonella. In the relevant experiment, three plates have each been processed at various doses of quinoline and subsequently the number of revertant colonies of TA98 Salmonella are measured; see Breslow (1984), Lunn *et al.* (2012).

For $i = 1, \dots, 6$ and $j = 1, 2, 3$, letting y_{ij} denote the number of colonies observed on plate j at dose x_i , the model considered (see Lunn *et al.* (2012)) is $y_{ij} \sim \text{Poisson}(\mu(x_i))$, where $\log(\mu_i) = \alpha + \beta + \gamma(x_i + 10) + \gamma x_i$. The priors for α, β, γ are independent zero-mean normal distributions with standard deviation 100.

We first consider an additive TCMC application to this problem, with the scaling constants in the additive transformation for α, β, γ being 0.21832, 0.056563 and 0.00024192, respectively. The forward and backward transformations are considered with equal probability. The rest of the details remain the same as in the Challenger problem. Quite encouraging TCMC convergence properties are indicated by our informal diagnostics. As before, μ and Σ are estimated from the stored 10^5 TCMC realizations, after ignoring the first 10^5 realizations as burn-in.

For application of our *iid* method, we set, for $d = 3$, $r_d = 3$, $a_d = 0.02$, and $M = 200$, as suggested by our experiments. Again, we avoided rejection sampling in the same way

as in the Challenger case, and considered $N_i = 5000$, drawing 10,000 realizations from the three-parameter posterior. The time for implementation here is only a minute.

Figure 12 compares TMCMC and *iid* sampling with respect to density estimation of the parameters with 10^5 TMCMC realizations thinned to 10,000 realizations by considering one in every 10. Once again, the *iid* results are in close agreement with the TMCMC results.

The estimated correlation structures, expectedly, are not much different with respect to the competing methods. The TMCMC estimates of the posterior correlations between (α, β) , (α, γ) and (β, γ) are -0.9627896 , 0.7810736 and -0.8901597 , respectively, while the respective *iid* estimates are -0.9625148 , 0.7774780 and -0.8887078 .

6.3 Application to the Rongelap Island dataset

We now consider application of our *iid* sampling idea to the challenging spatial statistics problem involving radionuclide count data on Rongelap Island. Following Diggle *et al.* (1998), we model the count data, for $i = 1, \dots, 157$, as

$$Y_i \sim \text{Poisson}(\mu_i),$$

where

$$\mu_i = t_i \exp\{\beta + S(\mathbf{x}_i)\},$$

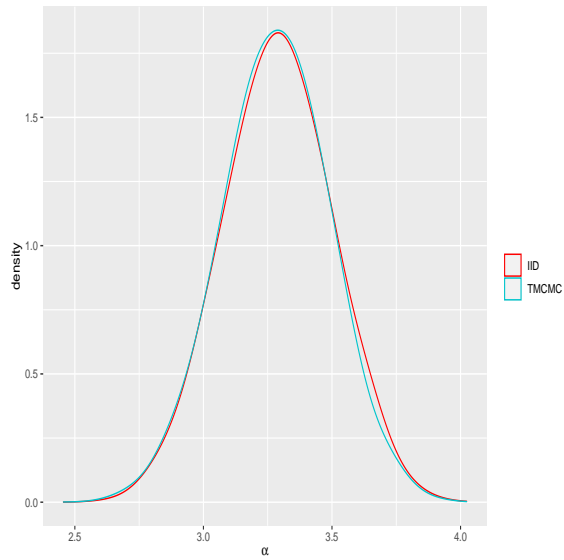
t_i being the duration of observation at location \mathbf{x}_i , β is an unknown parameter and $S(\cdot)$ is a zero-mean Gaussian process with isotropic covariance function of the form

$$\text{Cov}(S(\tilde{\mathbf{x}}_1), S(\tilde{\mathbf{x}}_2)) = \sigma^2 \exp\{-\alpha \|\tilde{\mathbf{x}}_1 - \tilde{\mathbf{x}}_2\|\}$$

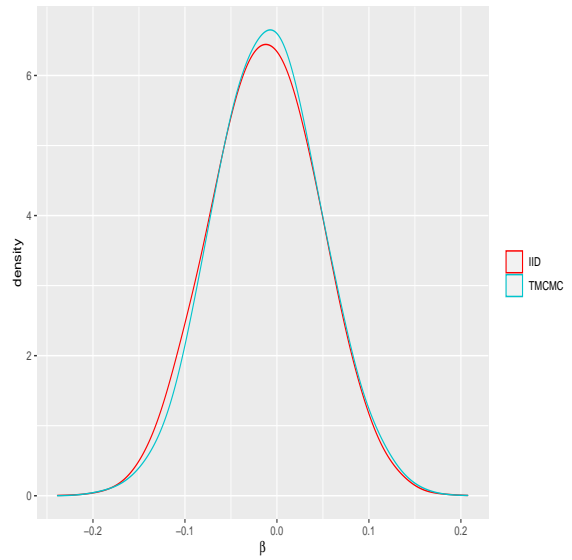
for any two locations $\tilde{\mathbf{x}}_1, \tilde{\mathbf{x}}_2$. In the above, (σ^2, α) are unknown parameters. We assume uniform priors on the entire parameter space corresponding to $(\beta, \log(\sigma^2), \log(\alpha))$. Since there are 157 latent Gaussian variables $S(\mathbf{x}_i)$ and three other unknowns $(\alpha, \beta, \sigma^2)$, there are in all 160 unknowns in this problem.

To first consider a TMCMC implementation, we adopted the same additive TMCMC sampler of Dey and Bhattacharya (2017) specific to this spatial count data problem (see Section 8 of their article), but also enhanced its convergence properties by adding the step with the flavour of Liu and Sabatti (2000) in the same way as in the previous applications regarding Challenger and Salmonella. After discarding the first 10^6 realizations as burn-in, we stored one in 100 in the next 10^6 iterations, to obtain 10,000 realizations, which we used for estimation of $\boldsymbol{\mu}$ and $\boldsymbol{\Sigma}$ needed for \mathbf{A}_i of our *iid* sampler. The TMCMC exercise took about 1 hour 40 minutes.

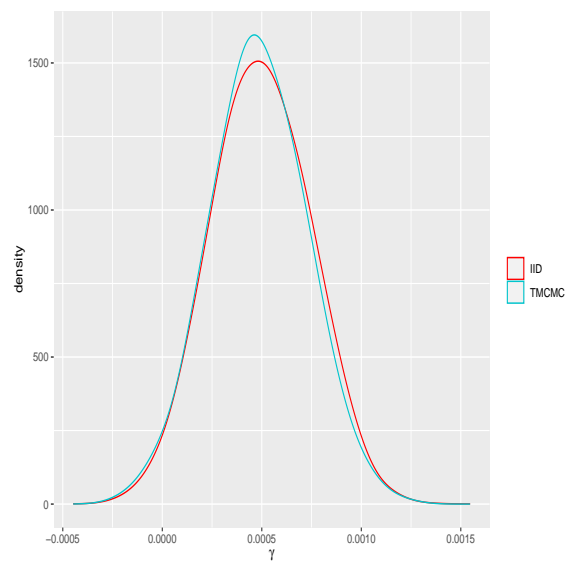
Now, with $d = 160$, application of the *iid* method requires appropriate specification of r_d and a_d such that \hat{p}_i are sufficiently large. However, in this challenging application, all our experiments failed to yield significant \hat{p}_i . To handle this challenge, we decided to flatten the posterior distribution in a way that its infimum and the supremum are reasonably close (so that \hat{p}_i are adequately large) on all the \mathbf{A}_i . This requires an appropriate flattening bijective transformation. As it turns out, the MCMC literature already contains instances of such transformations with stronger properties such that the transformation and its inverse are continuously differentiable. Such transformations are called diffeomorphisms. In fact, diffeomorphisms with stronger properties have been considered in Johnson and Geyer (2012); see also Dey and Bhattacharya (2016) who implement such diffeomorphisms in the TMCMC context. However, in the above works,



(a) TMCMC and *iid*-based density for α .



(b) TMCMC and *iid*-based density for β .



(c) TMCMC and *iid*-based density for γ .

Figure 12: Salmonella posterior. The red and blue colours denote the *iid* sample based density and the TMCMC based density, respectively.

the transformations are meant to reduce thick-tailed target distributions to thin-tailed ones. Here we need just the opposite; the Rongelap Island posterior needs to be converted to a thick-tailed distribution for our *iid* sampling purpose. As can be anticipated, the inverse transformations for thick to thin tail conversions will be appropriate here. Details follow.

6.3.1 A suitable diffeomorphic transformation and the related method

Observe that if $\pi_{\boldsymbol{\theta}}$, the multivariate target density of some random vector $\boldsymbol{\theta}$ is of interest, then

$$\pi_{\boldsymbol{\gamma}}(\boldsymbol{\gamma}) = \pi_{\boldsymbol{\theta}}(h(\boldsymbol{\gamma})) |\det \nabla h(\boldsymbol{\gamma})| \quad (25)$$

is the density of $\boldsymbol{\gamma} = h^{-1}(\boldsymbol{\theta})$, where h is a diffeomorphism. In the above, $\nabla h(\boldsymbol{\gamma})$ denotes the gradient of h at $\boldsymbol{\gamma}$ and $\det \nabla h(\boldsymbol{\gamma})$ stands for the determinant of the gradient of h at $\boldsymbol{\gamma}$.

[Johnson and Geyer \(2012\)](#) obtain conditions on h which make $\pi_{\boldsymbol{\gamma}}$ super-exponentially light. Specifically, they define the following isotropic function $h : \mathbb{R}^d \mapsto \mathbb{R}^d$:

$$h(\boldsymbol{\gamma}) = \begin{cases} f(\|\boldsymbol{\gamma}\|) \frac{\boldsymbol{\gamma}}{\|\boldsymbol{\gamma}\|}, & \boldsymbol{\gamma} \neq \mathbf{0} \\ 0, & \boldsymbol{\gamma} = \mathbf{0}, \end{cases} \quad (26)$$

for some function $f : (0, \infty) \mapsto (0, \infty)$. [Johnson and Geyer \(2012\)](#) confine attention to isotropic diffeomorphisms, that is, functions of the form h where both h and h^{-1} are continuously differentiable, with the further property that $\det \nabla h$ and $\det \nabla h^{-1}$ are also continuously differentiable. In particular, if $\pi_{\boldsymbol{\beta}}$ is only sub-exponentially light, then the following form of $f : [0, \infty) \mapsto [0, \infty)$ given by

$$f(x) = \begin{cases} e^{bx} - \frac{e}{3}, & x > \frac{1}{b} \\ x^3 \frac{b^3 e}{6} + x \frac{be}{2}, & x \leq \frac{1}{b}, \end{cases} \quad (27)$$

where $b > 0$, ensures that the transformed density $\pi_{\boldsymbol{\gamma}}$ of the form (25), is super-exponentially light.

In our current context, the $d = 160$ dimensional target distribution $\pi_{\boldsymbol{\theta}}$ needs to be converted to some thick-tailed distribution $\pi_{\boldsymbol{\gamma}}$. Hence, we apply the transformation $\boldsymbol{\gamma} = h(\boldsymbol{\theta})$, the inverse of the transformation considered in [Johnson and Geyer \(2012\)](#). Consequently, the density of $\boldsymbol{\gamma}$ here becomes

$$\pi_{\boldsymbol{\gamma}}(\boldsymbol{\gamma}) = \pi_{\boldsymbol{\theta}}(h^{-1}(\boldsymbol{\gamma})) |\det \nabla h(\boldsymbol{\gamma})|^{-1}, \quad (28)$$

where h is the same as (26) and f is given by (27). We also give the same transformation to the uniform proposal density (15), so that the new proposal density now becomes

$$q_i(\boldsymbol{\gamma}') = \frac{1}{\mathcal{L}(\mathbf{A}_i)} I_{\mathbf{A}_i}(h^{-1}(\boldsymbol{\gamma}')) |\det \nabla h(\boldsymbol{\gamma}')|^{-1}. \quad (29)$$

With (29) as the proposal density for (28), the proposal will not cancel in the acceptance ratio of the Metropolis-Hastings acceptance probability. For any set \mathbf{A} , let $h(\mathbf{A}) = \{h(\boldsymbol{\theta}) : \boldsymbol{\theta} \in \mathbf{A}\}$. Also, now let $s_i = \inf_{\boldsymbol{\gamma} \in h(\mathbf{A}_i)} \frac{\tilde{\pi}_{\boldsymbol{\gamma}}(\boldsymbol{\gamma})}{q_i(\boldsymbol{\gamma})}$ and $S_i = \sup_{\boldsymbol{\gamma} \in h(\mathbf{A}_i)} \frac{\tilde{\pi}_{\boldsymbol{\gamma}}(\boldsymbol{\gamma})}{q_i(\boldsymbol{\gamma})}$, where $\tilde{\pi}_{\boldsymbol{\gamma}}(\boldsymbol{\gamma})$ is

the same as (28) but without the normalizing constant. Then, with (29) as the proposal density we have

$$\begin{aligned} P_i(\boldsymbol{\gamma}, h(\mathbb{B} \cap \mathbf{A}_i)) &\geq \int_{h(\mathbb{B} \cap \mathbf{A}_i)} \min \left\{ 1, \frac{\tilde{\pi}_{\boldsymbol{\gamma}}(\boldsymbol{\gamma}')/q_i(\boldsymbol{\gamma}')}{\tilde{\pi}_{\boldsymbol{\gamma}}(\boldsymbol{\gamma})/q_i(\boldsymbol{\gamma})} \right\} q_i(\boldsymbol{\gamma}') d\boldsymbol{\gamma}' \\ &\geq p_i Q_i(h(\mathbb{B} \cap \mathbf{A}_i)), \end{aligned}$$

where $p_i = s_i/S_i$ and Q_i is the probability measure corresponding to (29). The rest of the details remain the same as before with necessary modifications pertaining to the new proposal density (29) and the new Metropolis-Hastings acceptance ratio with respect to (29) incorporated in the subsequent steps. Once $\boldsymbol{\gamma}$ is generated from (28) we transform it back to $\boldsymbol{\theta}$ using $\boldsymbol{\theta} = h^{-1}(\boldsymbol{\gamma})$.

6.3.2 Results with the diffeomorphic transformation

With the transformed posterior density corresponding to the form (25), our experiments suggested that $M = 10,000$, $b = 0.01$, $r_d = 7.8$ and $a_d = 0.0005$ are appropriate, and rendered \hat{p}_i significantly large for the transformed target. With $N_i = 5000$ and the technique of avoiding rejection sampling remaining the same as in the previous two applications, generation of 10,000 *iid* realizations took 30 minutes in our parallel processors.

Figures 13 and 14 show that the marginal density estimates with the TMCMC based and the *iid* based samples are in agreement, as in the previous examples. That the correlation structures obtained by both the methods are also in close agreement, is borne out by Figure 15.

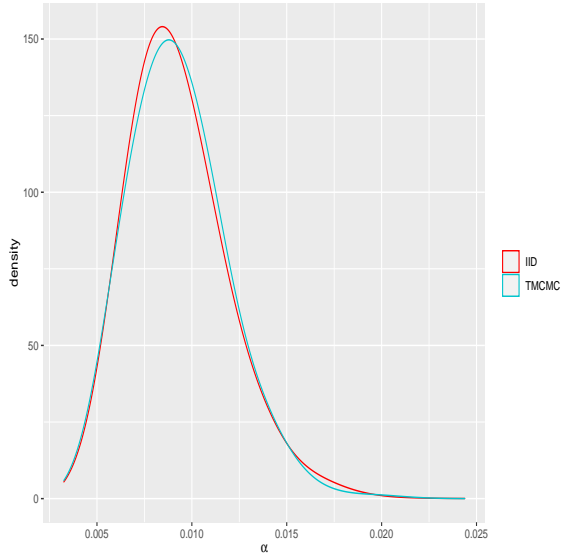
7 Summary and conclusion

In this article, we have proposed a general methodology for producing *iid* realizations from any distribution on \mathbb{R}^d , for arbitrary $d \geq 1$. Our key idea is to represent the target distribution as an infinite mixture of component distributions defined on a central ellipsoid and on successive ellipsoidal annuli. The compactness of these sets allowed us to establish a minorization inequality for the Metropolis-Hastings algorithm with uniform proposals, which in turn facilitated a tractable perfect sampling scheme.

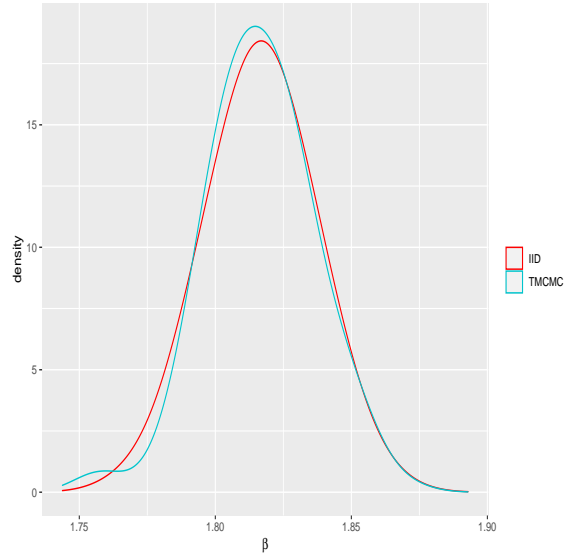
By integrating these results, we developed a generic parallel algorithm for exact *iid* sampling from general target distributions. Our approach is simple, widely applicable, and avoids the computational burden of coupling from the past. It also scales naturally with modern parallel computing environments.

Through experiments, we demonstrated that the method performs effectively on a variety of challenging problems, including high-dimensional settings and complex posterior distributions. In particular, we showed that 10,000 *iid* realizations can be generated quickly and reliably, even in dimensions as high as 160.

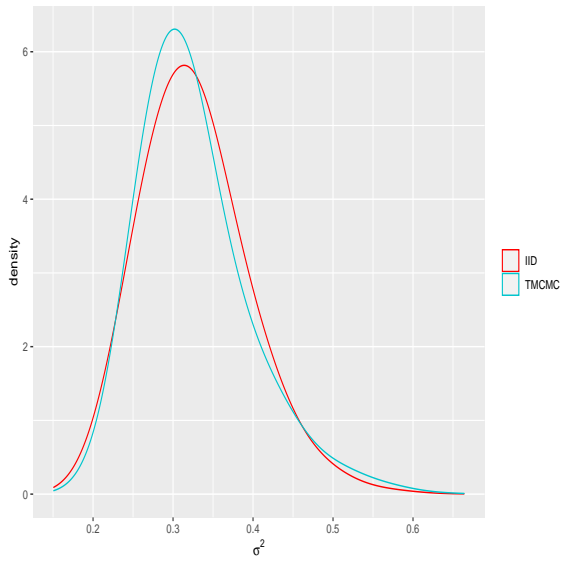
The impact of this foundational work has been substantial, spawning a sequence of subsequent developments that extend the *iid* sampling methodology to increasingly challenging contexts. [Bhattacharya \(2021b\)](#) extended the method to general multimodal and variable-dimensional distributions, illustrating its applicability on mixtures of 50-dimensional normals and variable-dimensional normal mixtures for the acidity dataset. The methodology was further extended to doubly intractable posterior distributions,



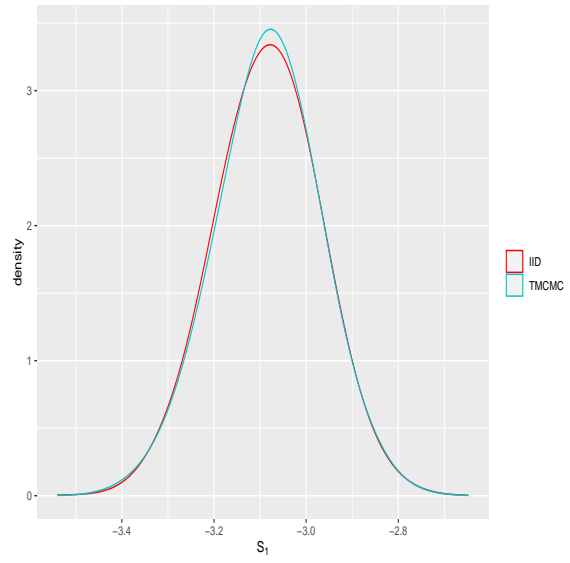
(a) TCMC and *iid*-based density for α .



(b) TCMC and *iid*-based density for β .

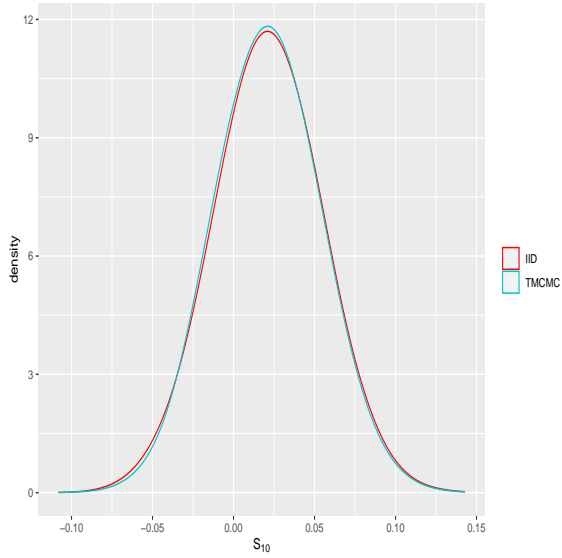


(c) TCMC and *iid*-based density for σ^2 .

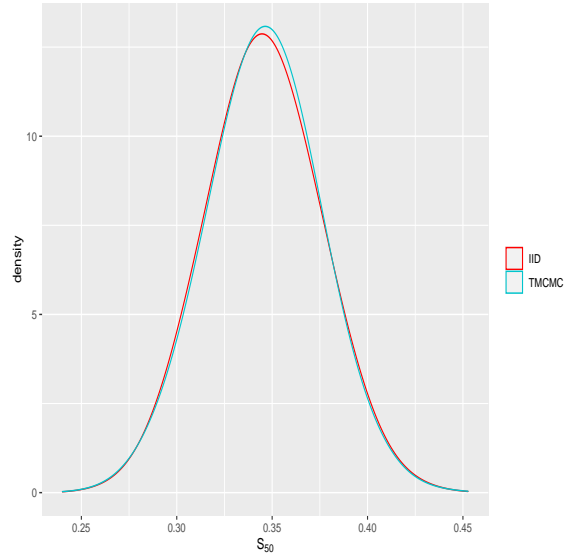


(d) TCMC and *iid*-based density for S_1 .

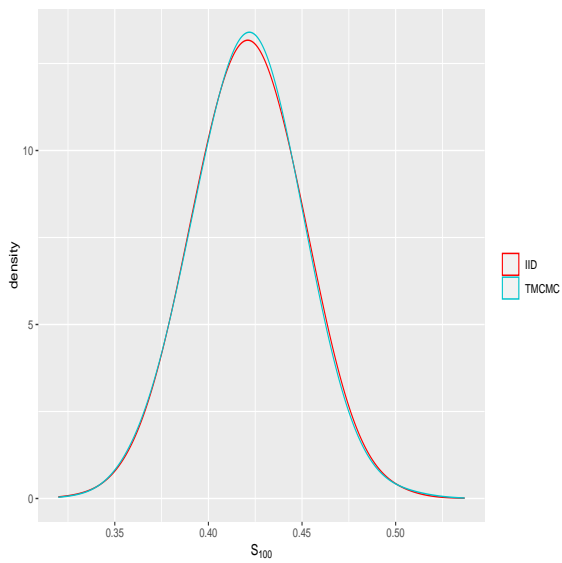
Figure 13: Rongelap Island posterior. The red and blue colours denote the *iid* sample based density and the TCMC based density, respectively.



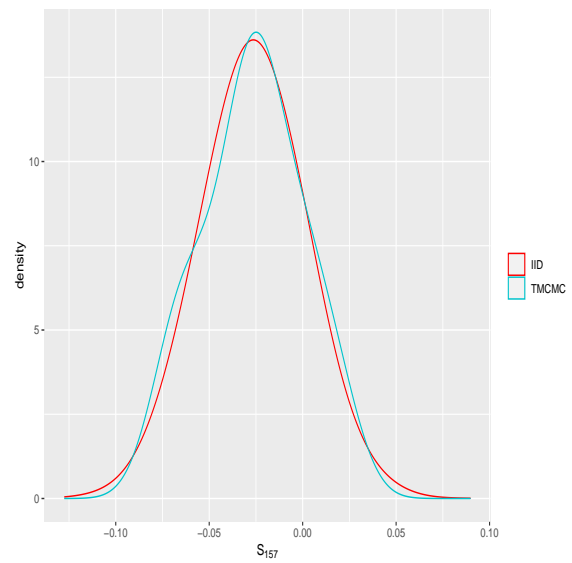
(a) TMCMC and *iid*-based density for S_{10} .



(b) TMCMC and *iid*-based density for S_{50} .

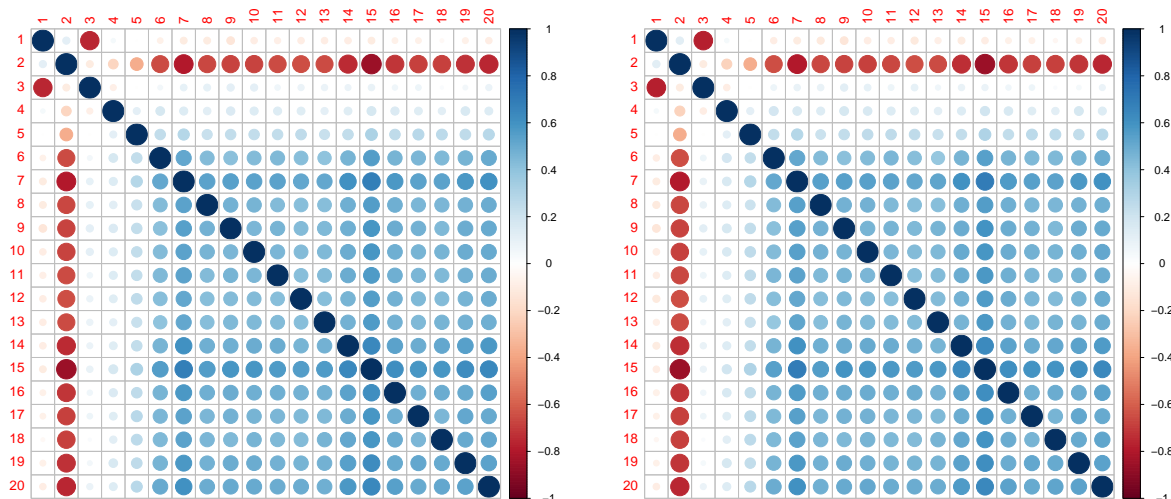


(c) TMCMC and *iid*-based density for S_{100} .



(d) TMCMC and *iid*-based density for S_{157} .

Figure 14: Rongelap Island posterior. The red and blue colours denote the *iid* sample based density and the TMCMC based density, respectively.



(a) TCMCM based correlation structure.

(b) Correlation structure based on *iid* samples.

Figure 15: Rongelap Island posterior. TCMCM and *iid*-based correlation structures for the first 20 co-ordinates.

where normalizing constants depend on parameters and are analytically intractable. By combining Monte Carlo and importance sampling approximations with Gaussian process interpolations, the *iid* sampling framework achieved highly accurate and efficient sampling for complex posteriors, including two-dimensional Ising and Strauss models, two-dimensional normal-gamma posteriors, and a 100-dimensional autologistic model (Bhattacharya (2021a)). The work was further extended to the framework of Bayesian nonparametrics, enabling exact *iid* sampling from Dirichlet process mixture posteriors—a class of distributions notoriously difficult to sample satisfactorily using MCMC methods due to their infinite-dimensional and discrete nature. The *iid* sampling method was validated using the novel and efficient Dirichlet process mixture setup of Bhattacharya (2008) on benchmark datasets such as enzyme, acidity, and galaxy data, demonstrating both computational efficiency and accuracy, with 10,000 *iid* realizations generated in minutes using parallel computing (Bhattacharya (2022)). Most recently, Bhattacharya *et al.* (2025) extended the *iid* sampling procedure to a novel Bayesian nonparametrics theory based on random normalizing flows. Such flows, governed by random diffeomorphisms, are induced by compositions of monotone Gaussian processes, leading to highly complex, non-standard distributions on non-Euclidean spaces. Implementation of the *iid* sampling theory in such a setup, along with its comparison with MCMC, emphatically brought out the convergence challenges of the latter in high dimensions and the necessity of *iid* sampling.

Together, these developments underscore the versatility and power of the *iid* sampling methodology. They illustrate a coherent trajectory of research that extends the original framework from high-dimensional Euclidean distributions to doubly intractable distributions and nonparametric Bayesian posteriors. This body of work provides a practical and theoretically rigorous solution to exact *iid* sampling, offering promising directions for both theoretical research and applied Bayesian computation, particularly in contexts

where assessing convergence of MCMC methods is difficult.

Acknowledgments

We are sincerely grateful to the Editors for very valuable feedback. We also thank ChatGPT for some help with proofreading.

Bibliography

- Bhattacharya, D., Roy, S., and Bhattacharya, S. (2025). Bayesian Nonparametrics With Random Normalizing Flows. Available at https://www.researchgate.net/publication/395337211_Bayesian_Nonparametrics_With_Random_Normalizing_Flows.
- Bhattacharya, S. (2008). Gibbs Sampling Based Bayesian Analysis of Mixtures with Unknown Number of Components. *Sankhya. Series B*, **70**, 133–155.
- Bhattacharya, S. (2021a). IID Sampling from Doubly Intractable Distributions. arXiv:2112.07939v1.
- Bhattacharya, S. (2021b). IID Sampling from Intractable Multimodal and Variable-Dimensional Distributions. arXiv:2109.12633v2.
- Bhattacharya, S. (2022). IID Sampling from Posterior Dirichlet Process Mixtures. arXiv:2206.09233v1.
- Breslow, N. (1984). Extra-Poisson Variation in Log-Linear Models. *Applied Statistics*, **33**, 38–44.
- Christensen, O. F. (2004). Monte Carlo Maximum Likelihood in Model-Based Geostatistics. *Journal of Computational and Graphical Statistics*, **13**, 702–718.
- Christensen, O. F. (2006). Robust Markov Chain Monte Carlo Methods for Spatial Generalized Linear Mixed Models. *Journal of Computational and Graphical Statistics*, **15**, 1–17.
- Dalal, S. R., Fowlkes, E. B., and Hoadley, B. (1989). Risk Analysis of the Space Shuttle: pre-Challenger Prediction of Failure. *Journal of the American Statistical Association*, **84**, 945–957.
- Dey, K. K. and Bhattacharya, S. (2016). On Geometric Ergodicity of Additive and Multiplicative Transformation Based Markov Chain Monte Carlo in High Dimensions.

- Brazilian Journal of Probability and Statistics*, **30**, 570–613. Also available at “<http://arxiv.org/pdf/1312.0915.pdf>”.
- Dey, K. K. and Bhattacharya, S. (2017). A Brief Tutorial on Transformation Based Markov Chain Monte Carlo and Optimal Scaling of the Additive Transformation. *Brazilian Journal of Probability and Statistics*, **31**, 569–617. Also available at “<http://arxiv.org/abs/1307.1446>”.
- Diggle, P. J., Tawn, J. A., and Moyeed, R. A. (1997). Geostatistical Analysis of Residual Contamination from Nuclear Weapons Testing. In V. Barnett and K. F. Turkman, editors, *Statistics for Environment 3: Pollution Assessment and Control*, pages 89–107. Chichester: Wiley.
- Diggle, P. J., Tawn, J. A., and Moyeed, R. A. (1998). Model-Based Geostatistics (with discussion). *Applied Statistics*, **47**, 299–350.
- Dutta, S. and Bhattacharya, S. (2014). Markov Chain Monte Carlo Based on Deterministic Transformations. *Statistical Methodology*, **16**, 100–116. Also available at <http://arxiv.org/abs/1106.5850>. Supplement available at <http://arxiv.org/abs/1306.6684>.
- Giraud, C. (2015). *Introduction to High-Dimensional Statistics*. CRC Press, Boca Raton, FL.
- Johnson, L. T. and Geyer (2012). Variable Transformation to Obtain Geometric Ergodicity in the Random-Walk Metropolis Algorithm. *The Annals of Statistics*, **40**, 3050–3076.
- Liu, J. S. and Sabatti, S. (2000). Generalized Gibbs Sampler and Multigrid Monte Carlo for Bayesian Computation. *Biometrika*, **87**, 353–369.
- Lunn, D., Jackson, C., Best, N., Thomas, A., and Spiegelhalter, D. (2012). *The BUGS Book: A Practical Introduction to Bayesian Analysis*. CRC Press, Boca Raton, Florida.
- Martz, H. F. and Zimmer, W. J. (1992). The Risk of Catastrophic Failure of the Solid Rocket Boosters on the Space Shuttle. *The American Statistician*, **46**, 42–47.
- Mukhopadhyay, S. and Bhattacharya, S. (2012). Perfect Simulation for Mixtures with Known and Unknown Number of Components. *Bayesian Analysis*, **7**, 675–714.
- Murdoch, D. and Green, P. J. (1998). Exact sampling for a continuous state. *Scandinavian Journal of Statistics*, **25**, 483–502.

- Propp, J. G. and Wilson, D. B. (1996). Exact Sampling with Coupled Markov Chains and Applications to Statistical Mechanics. *Random Structures and Algorithms*, **9**, 223–252.
- Robert, C. P. and Casella, G. (2004). *Monte Carlo Statistical Methods*. Springer-Verlag, New York.
- Rue, H. (2001). Fast sampling of Gaussian Markov random fields. *Journal of the Royal Statistical Society. Series B*, **63**, 325–338.